JOURNAL OF COMPUTATIONAL PHYSICS 104, 377–397 (1993)

A Treatment of Discontinuities for Finite Difference Methods in the Two-Dimensional Case

DE-KANG MAO*

Department of Mathematics, University of California, Los Angeles, California 90024 and
Department of Mathematics, Shanghai University of Science and Technology, Shanghai, People's Republic of China

Received January 29, 1991; revised August 27, 1991

This paper extends the treatment of discontinuities introduced by the author in [13], [14], and [15] to the two dimensional case. The main idea relies on the fact that on each side of a discontinuity the computations draw information from the same side. A numerical method for ordinary differential equations modeling the movement of the discontinuity curve is incorporated into the algorithm to compute discontinuity positions. The conservation feature of the treatment is studied for the case of an isolated discontinuity. Finally, we study two-dimensional scalar systems and systems of conservation laws and display some numerical results when our treatment is applied.

1. INTRODUCTION

Front-tracking methods are distinguished from capturing methods by the choice of a lower adaptive grid, the so-called front or interface, to fit the discontinuity occurring in the solution. This front (either a point or a curve in 1D or 2D, respectively) is associated with physical waves in the solution. It is implicitly defined from the solution and evolves dynamically with it. Eearly proposals for front tracking are described in Richtmyer and Morton [20], and its realizations in one space dimension can be found in [11, 16, 20, 22]. A more challenging task is its realization in two space dimensions due to geometric and dynamic complications. Since 1980, J. Glimm and his coworkers have done extensive work to develop two-dimensional front tracking methods and applied them to different problems of fluid dynamics (see [2, 3–8, 9]).

In [13–15] we develop a front tracking technique in the one-dimensional case, which is called the treatment of discontinuities, and apply it to conservative difference schemes. Its main idea is that in the field of the discontinuity the computation only uses information from the same side of the discontinuity. In the scalar case, this is done by doing the following: at the grid points located on the other side of the discontinuity, we replace the original data by its extrapolated values from the other side, which are used in the numerical fluxes. In the system case, Riemann problems related to the original and extrapolated data are solved to obtain the data which replace the original data. By doing this, we do not have flow states on the discontinuity fronts. Instead, the whole computation of the numerical solution still proceeds on the regular grid, and the algorithm is much simpler than that of other one-dimensional front tracking methods. Also, several special treatments have been developed to handle the interactions of discontinuities. Moreover, the conservation feature of the treatment has been studied.

In this paper we extend the treatment developed in [13] to two space dimensions. We first want that the two-dimensional extension has no flow states on discontinuity fronts and then that the computation of the numerical solution proceeds on the regular grid. We also want the extension to be as much dimension-by dimension as possible.

The paper is organized in the following manner: Section 2 briefly recalls the treatment in one space dimension; Section 3 describes the treatment for an isolated discontinuity; Section 4 discusses the conservation feature of the treatment for an isolated discontinuity and shows that in the two-dimensional scalar case the numerical solution is almost conserved. Section 5 describes the treatment of interactions of discontinuities; Section 6 describes the programming of the algorithm; and Section 7 displays some numerical examples of the treatment.

2. BRIEF RECALL OF THE TREATMENT FOR ONE SPACE DIMENSION

In this section, we briefly recall the treatment in the one space dimension introduced in [13]. The partial differential equation under concern is

$$u_t + f(u)_x = 0 \tag{2.1a}$$

* Research was supported by ONR Grant No. N00014-86-k-0691.

0021-9991/93 $5.00

with the initial condition

$$u(x, 0) = u_0(x), \tag{2.1b}$$

where both u and f are vectors. Assume that the underlying finite difference scheme is a general conservative scheme:

$$u_j^{n+1} = u_j^n - \lambda(\hat{f}_{j+1/2}^n - \hat{f}_{j-1/2}^n), \tag{2.2}$$

where u_j^n denotes the numerical solution at the grid point (x_j, t^n),

$$\hat{f}_{j+1/2}^n = \hat{f}(u_{j-k+1}^n, ..., u_{j+k}^n) \tag{2.3}$$

is a consistent numerical flux depending on $2k$ variables, $\lambda = \tau/h$ is the mesh ratio, and τ and h are the time and space increments, respectively.

We denote the grid cells that contain discontinuities as the critical cells. For an isolated discontinuity, when (2.1) is scalar, the treatment is carried out generally as in the four steps below:

(1) Extrapolate the numerical solution from each side of the discontinuity to the opposite side, thereby obtaining a set of extrapolated data:

$$u_{j_1-k}^{n,+}, ..., u_{j_1}^{n,+}, u_{j_1+1}^{n,-}, ..., u_{j_1+k+1}^{n,-}, \tag{2.4}$$

where $[x_{j_1}, x_{j_1+1}]$ is the critical cell, the data with "$-$" come from extrapolation from the left to the right, and the data with "$+$" are just reversed (see Fig. 2.1).

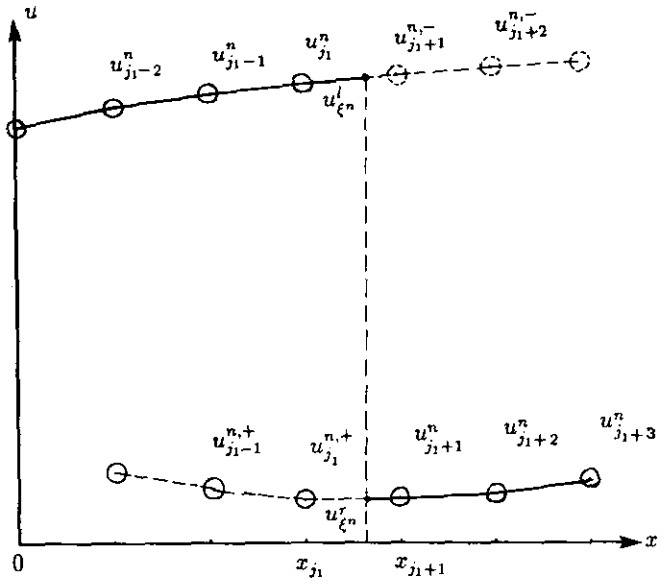

FIG. 2.1. The numerical solution at the nth level has an isolated discontinuity in the critical cell $[x_{j_1}, x_{j_1+1}]$, on each side of which the numerical solution is smooth. ξ^n is the discontinuity position in the critical cell. The numerical solution is extrapolated from each side to the opposite side to obtain a set of extrapolated data.

(2) Compute the numerical solution on each side of the discontinuity at the new level by using the extrapolated data from the same side. That is, when $x_j \leqslant x_{j_1}$,

$$u_j^{n+1} = u_j^n - \lambda(\hat{f}_{j+1/2}^{n,-} - \hat{f}_{j-1/2}^{n,-}), \tag{2.5}$$

where

$$\hat{f}_{j+1/2}^{n,-} = \hat{f}(u_{j-k+1}^n, ..., u_{j_1}^n, u_{j_1+1}^{n,-}, ..., u_{j+k}^{n,-}), \tag{2.6}$$

and when $x_j > x_{j_1}$,

$$u_j^{n+1} = u_j^n - \lambda(\hat{f}_{j+1/2}^{n,+} - \hat{f}_{j-1/2}^{n,+}), \tag{2.7}$$

where

$$\hat{f}_{j+1/2}^{n,+} = \hat{f}(u_{j-k+1}^{n,+}, ..., u_{j_1}^{n,+}, u_{j_1+1}^n, ..., u_{j_1+k}^n). \tag{2.8}$$

(3) Compute ξ^{n+1}, the discontinuity position at the new level by discretizing the Hugoniot condition. For example, it can be

$$\xi^{n+1} = \xi^n + \frac{f(u_{\xi^n}^r) - f(u_{\xi^n}^l)}{u_{\xi^n}^r - u_{\xi^n}^l}\tau, \tag{2.9}$$

where ξ^n is the discontinuity position at the level n, and $u_{\xi^n}^l$ and $u_{\xi^n}^r$ are the extrapolated data of the numerical solution from the two sides at location ξ^n.

(4) Set the critical cell for the new level according to the new position of the discontinuity. If ξ^{n+1} remains in $[x_{j_1}, x_{j_1+1}]$, the same cell will be the critical cell at the new level. If ξ^{n+1} moves into one of the adjacent cells, then this cell becomes the new critical cell, and the numerical solution computed at the grid point crossed by the discontinuity are updated by the extrapolated data appropriately.

When (2.1) is a system of equations, the treatment is still carried out in four steps. However, Riemann problems related to the original and extrapolated data are solved and proper states are chosen as the data on the opposite side of the discontinuity in the computation of the numerical solution. For example, to compute the data that will replace the right side, original data for the left side numerical fluxes in step (2), we solve the Riemann problems related to $u_{i_1+1}^{n,-}$ and $u_{i_1+1}^n$, $u_{i_1+2}^{n,-}$ and $u_{i_1+2}^n$, ... If the discontinuity is a left shock, we pick the extrapolated data; if the discontinuity is a right shock, we pick the right middle states; and if the discontinuity is a contact discontinuity, we pick the left middle states. In doing so, the treatment only affects the field of the discontinuity.

Several techniques have been developed to handle the interactions of discontinuities. Among them is a so-called "stacking treatment" which deals with the critical cells stacking in the same grid cell (see [13]).

3. TREATMENT OF ISOLATED DISCONTINUITIES IN TWO SPACE DIMENSIONS

In this section we describe the treatment of isolated discontinuities in two space dimensions. The equation under concern is

$$u_t + f(u)_x + g(u)_y = 0 \tag{3.1a}$$

with the initial condition

$$u(x, y, 0) = u_0(x, y), \tag{3.1b}$$

where all u, u_0, f, and g are scalar.

We first need to extend the concept of a critical cell to the two-dimensional case. The critical intervals are those that interact with the discontinuity curve (refer to Fig. 3.1). There are two types of critical intervals, the horizontal critical intervals on horizontal grid lines and the vertical critical intervals on vertical grid lines. A discontinuity in the numerical solution is represented by a sequence of horizontal and vertical critical intervals; all of them contain an intersection point of the discontinuity curve and a grid line. We denote these interaction points as the discontinuity positions.

For an isolated discontinuity, the treatment is still carried out generally in four steps as in the one-dimensional case described in Section 2, i.e.,

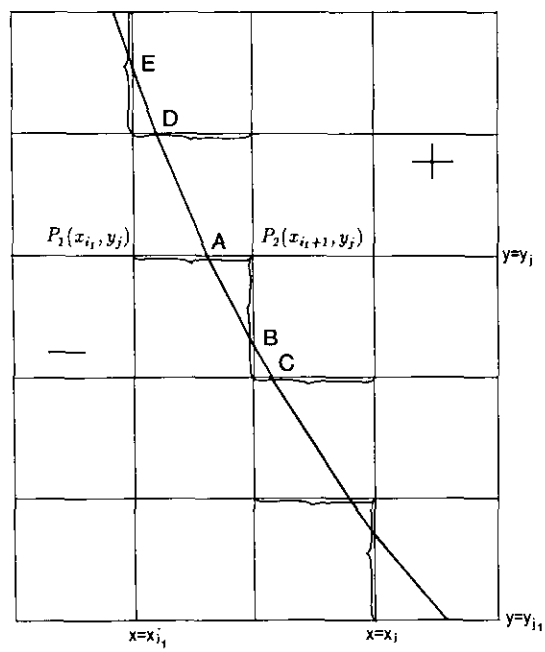

FIG. 3.1. Discontinuity curve C is represented by a group of critical intervals, which are indicated by horizontal and vertical braces. A, B, C, ... are discontinuity positions in the critical mesh intervals. The two sides of the numerical solution separated by C are denoted by "$-$" and "$+$," respectively.

(1) compute the data that will replace the original data on the other side of the discontinuity;

(2) compute the numerical solution on each side of the discontinuity;

(3) compute discontinuity positions at the new level by discretizing the Hugoniot condition;

(4) set the critical intervals at the new level according to the new discontinuity positions and update the numerical solution at grid points that the discontinuity crosses.

However, due to geometric and physical difficulties, the two-dimensional treatment is more complicated than its one-dimensional version. In the following subsections, we shall address these difficulties and describe how we shall overcome them. From Subsection 1 through Subsection 7, we shall only study the scalar case, while in Subsection 8 we shall extend the treatment to Euler's equations of gas dynamics.

1. *The Underlying Schemes*

We choose as underlying schemes the predictor–corrector methods of lines approximating (3.1) (see [17–19, 21] for the methods of lines), i.e.,

$$\begin{aligned} u_{i,j}^{n+1/2} &= u_{i,j}^n - L_{\hat f}(\mathbf{u}^n)_{i,j} - L_{\hat g}(\mathbf{u}^n)_{i,j} && \text{(predictor)} \\ \tilde u_{i,j}^{n+1} &= u_{i,j}^{n+1/2} - L_{\hat f}(\mathbf{u}^{n+1/2})_{i,j} \\ &\quad - L_{\hat g}(\mathbf{u}^{n+1/2})_{i,j} && \text{(corrector)}, \\ u_{i,j}^{n+1} &= \tfrac{1}{2}(u_{i,j}^n + \tilde u_{i,j}^{n+1}), \end{aligned} \tag{3.2}$$

where

$$\begin{aligned} L_{\hat f}(\mathbf{u}^n)_{i,j} &= \frac{\lambda}{2}(\hat f_{i+1/2,j}^n - \hat f_{i-1/2,j}^n) \\ L_{\hat g}(\mathbf{u}^n)_{i,j} &= \frac{\lambda}{2}(\hat g_{i,j+1/2}^n - \hat g_{i,j-1/2}^n) \end{aligned} \tag{3.3}$$

are approximations to $\frac{1}{2}\tau f_x$ and $\frac{1}{2}\tau g_x$ at the point (i, j), with the fluxes $f_{i+1/2,j}^n$ and $g_{i,j+1/2}^n$ defined as

$$\begin{aligned} \hat f_{i+1/2,j}^n &= \hat f(u_{i-k+1,j}^n, \ldots, u_{i+k,j}^n) \\ \hat g_{i,j+1/2}^n &= \hat g(u_{i,j-k+1}^n, \ldots, u_{i,j+k}^n) \end{aligned} \tag{3.4}$$

which are consistent in the sense that

$$\begin{aligned} \hat f(u, \ldots, u) &= f(u) \\ \hat g(u, \ldots, u) &= g(u). \end{aligned} \tag{3.5}$$

We would like to point out that the discussion in this paper applies to any types of Runge–Kutta methods for lines as well.

The reason for choosing this type of difference schemes as underlying schemes is that we can avoid two-dimensional extrapolation and still obtain second-order accuracy for both the numerical solution and the discontinuity positions. This will be shown in the sequel.

Since the underlying scheme is essentially a combination of two forward Euler schemes,

$$u_{i,j}^{n+1} = u_{i,j}^n - \frac{\lambda}{2}(\hat{f}_{i+1/2,j}^n - \hat{f}_{i-1/2,j}^n) - \frac{\lambda}{2}(\hat{g}_{i,j+1/2}^n - \hat{g}_{i,j-1/2}^n), \tag{3.6}$$

it is sufficient to build up the treatment in the case of the forward Euler method.

2. *Implementations of Step* 1 *and Step* 2

Denote with "$-$" and "$+$" the two parts of the (x, t)-plane separated by the isolated discontinuity, as shown in Fig. 3.1. We prepare the extrapolated data in step (1) as follows: For a horizontal critical interval, extrapolate the numerical solution along the x direction, and for a vertical critical interval, extrapolate the numerical solution along the y direction. In doing so, we obtain two sets of extrapolated data, i.e., the extrapolated data along the x direction with a subscript "x" and the extrapolated data along the y direction with a subscript "y."

In Step (2), we replace the original data on the opposite side of the discontinuity by the extrapolated data obtained above in the numerical fluxes. For example, the numerical solution evaluated at the point $P_1(x_{i_1}, y_j)$, which belongs to the "$-$" side, is computed as

$$u_{i_1,j}^{n+1} = u_{i_1,j}^n - \frac{\lambda}{2}(\hat{f}_{i_1+1/2,j}^{n,-} - \hat{f}_{i_1-1/2,j}^{n,-}) - \frac{\lambda}{2}(\hat{g}_{i_1,j+1/2}^{n,-} - \hat{g}_{i_1,j-1/2}^{n,-}), \tag{3.7}$$

where

$$\hat{f}_{i+1/2,j}^{n,-} = \hat{f}(u_{i-k+1,j}^n, \ldots, u_{i_1,j}^n, u_{x,i_1+1,j}^{n,-}, \ldots, u_{x,i+k,j}^{n,-}) \tag{3.8}$$

and

$$\hat{g}_{i_1,j+1/2}^{n,-} = \hat{g}(u_{i_1,j-k+1}^n, \ldots, u_{i_1,j+1}^n, u_{y,i_1,j+2}^{n,-}, \ldots, u_{y,i_1,j+k}^{n,-}), \tag{3.9}$$

and the data indexed with "$-$" are extrapolated data from the "$-$" side to the "$+$" side. For another example, the numerical solution at the point $P_2(x_{i_1+1}, y_j)$, which belongs to the "$+$" side, is computed as

$$u_{i_1+1,j}^{n+1} = u_{i_1+1,j}^n - \frac{\lambda}{2}(\hat{f}_{i_1+3/2,j}^{n,+} - \hat{f}_{i_1+1/2,j}^{n,+}) - \frac{\lambda}{2}(\hat{g}_{i_1+1,j+1/2}^{n,+} - \hat{g}_{i_1+1,j-1/2}^{n,+}), \tag{3.10}$$

where

$$\hat{f}_{i+1/2,j}^{n,+} = \hat{f}(u_{x,i-k+1,j}^{n,+}, \ldots, u_{x,i_1,j}^{n,+}, u_{i_1+1,j}^n, \ldots, u_{i+k,j}^n) \tag{3.11}$$

and

$$\hat{g}_{i_1+1,j+1/2}^{n,+} = \hat{g}(u_{y,i_1+1,j-k+1}^{n,+}, \ldots, u_{y,i_1+1,j-1}^{n,+}, u_{i_1+1,j}^n, \ldots, u_{i_1+1,j+k}^n), \tag{3.12}$$

and the data indexed with "$+$" are extrapolated data from the "$+$" side to the "$-$" side. In doing so, the computation on each side of the discontinuity uses only information from the same side.

Since all the parameters in $\hat{f}$ or $\hat{g}$ are on the same horizontal or vertical grid line, we do not require extrapolated data along diagonal directions. This is the benefit of using this type of underlying schemes; otherwise, two-dimensional extrapolation will be involved.

Because the extrapolated data are obtained in such a dimension-by-dimension fashion, the extrapolated data at the same point obtained from different directions are different. Therefore, different extrapolated data will be used at the same grid points in the computation. Nevertheless, the numerical experiments show that this does not produce problems. The reason is that these extrapolated data are essentially "virtual" to the computation since shocks have a characteristic-converging feature and contact discontinuities have a characteristic-paralleling feature, by which the solution on each side of the discontinuity substantially obtains information only from the same side.

3. *Computing Discontinuity Positions*

The implementation of step (3), i.e., computing discontinuity positions, is easy for the one-dimensional case, since the Hugoniot condition in that case is an ordinary differential equation. However, it is complicated for the two-dimensional case since the Hugoniot condition is now a partial differential equation involving the normal vector to the discontinuity curve (see [23]). If we discretize the Hugoniot condition along the normal direction in order to compute the discontintuity positions, just as is done in most tracking methods, the discontinuity positions will go to the insides of the grid cells at the following level. Hence, it is difficult to maintain the computation on the regular grid.

In this paper we discretize the Hugoniot condition along the horizontal and vertical directions, instead of the normal directions. We compute the local horizontal and vertical velocities of the discrete discontinuity positions and use them to track the discontinuity positions along the grid lines. In doing so, we need no information about the numerical solution inside the grid cells.

The following theorem, which is derived from the Hugoniot condition, gives the formulae to calculate these two velocities.

THEOREM 2.1. *On the (x, y)-plane, an intersection point of a discontinuity curve of* (1.1) *with a horizontal line satisfies the ordinary differential equation*

$$\frac{\partial x}{\partial t} = \frac{\alpha[f] + \beta[g]}{\alpha[u]}, \tag{3.13}$$

and an intersection point of the discontinuity curve with a vertical line satisfies

$$\frac{\partial y}{\partial t} = \frac{\alpha[f] + \beta[g]}{\beta[u]}, \tag{3.14}$$

where x and y are the coordinates of the intersection point, $[v]$ indicates the jump of the quantity v across the discontinuity, and (α, β) is the normal vector to the discontinuity curve at the intersection point.

Proof. Assume S is a discontinuity surface of (3.1a) in the three-dimensional (x, y, t)-space, which cuts a horizontal plane at time t by a curve C (see Fig. 3.2). At a point p on C, the two states separated by the discontinuity satisfy the Hugoniot condition

$$\mathbf{n} \cdot ([u], [f], [g]) = 0, \tag{3.15}$$

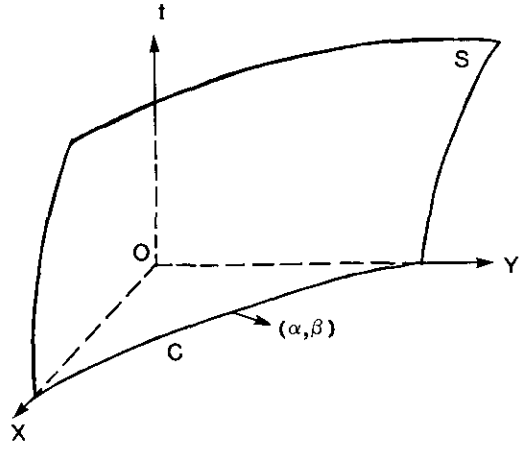

FIG. 3.2. Discontinuity surface S cuts a horizontal plane by a curve C, (α, β) is the horizontal normal to S at p.

where $\mathbf{n}$ is the normal vector to S at p (see [23]). This also means that the vector $\mathbf{v}_1 = ([u], [f], [g])$ is tangential to S. Since the horizontal normal vector to C at p on the (x, y)-plane is (α, β), the vector $\mathbf{v}_2 = (0, -\beta, \alpha)$ is also tangential to S. Therefore, the vector

$$\mathbf{v}_1 \times \mathbf{v}_2 = (-\alpha[f] - \beta[g], \alpha[u], \beta[u]) \tag{3.16}$$

is perpendicular to S at p. This indicates that S has the differential form

$$(\alpha[f] + \beta[g])\, dt = \alpha[u]\, dx + \beta[u]\, dy. \tag{3.17}$$

By taking x and y to be constants, we obtain (3.13) and (3.14). This completes the proof.

4. *Calculation of Normal Vectors*

The normal vector (α, β) is required in computing the discontinuity position. This can be numerically computed by interpolating nearby discontinuity positions. Assume that A is a position of the discontinuity in a horizontal critical interval (as shown in Fig. 3.1). If choosing (A, B) as the interpolation stencil, one can compute (α, β) with first-order accuracy as

$$\begin{aligned} \alpha &= -\frac{y_A - y_B}{r_{AB}} \\ \beta &= \frac{x_A - x_B}{r_{AB}}, \end{aligned} \tag{3.18}$$

where (x_A, y_A) and (x_B, y_B) are the coordinates of points A and B, and r_{AB} is the distance between A and B, i.e.,

$$r_{AB} = ((x_A - x_B)^2 + (y_A - y_B)^2)^{1/2}.$$

If choosing (A, B, C) as the interpolation stencil, one can compute (α, β) with second-order accuracy as

$$\begin{aligned} \alpha &= -\left(r_{AC} \frac{y_A - y_B}{r_{AB}} - r_{AB} \frac{y_A - y_C}{r_{AC}} \right) \Big/ (r_{AC} - r_{AB}) \\ \beta &= \left(r_{AC} \frac{x_A - x_B}{r_{AB}} - r_{AB} \frac{x_A - x_C}{r_{AC}} \right) \Big/ (r_{AC} - r_{AB}). \end{aligned} \tag{3.19}$$

However, the choice of the interpolation stencils is critical to the stability of the method. Numerical experiments show that arbitrary choice of the stencils, for example, picking positions symmetrically on the left- and right-hand sides of A, may produce wiggles in the discontinuity curve and finally spoil the whole computation. In this subsection, we will give a so-called "upwind" way for choosing the interpolation stencils, which will keep the computation stable.

According to (3.15), the movement of a discontinuity curve of (3.1) at each point is a combination of two movements, a horizontal displacement with speed $[f]/[u]$ and a vertical one with speed $[g]/[u]$. Based on this observation, the interpolation stencils can be chosen in an upwind way. For example, to compute the normal vector at point A, we first evaluate $s_A = (g(u_A^r) - g(u_A^l))/(u_A^r - u_A^l)$, which is an approximation to $[g]/[u]$ at A, where u_A^l and u_A^r are the extrapolated data from the left and right sides along the x direction at point A. If $s_A > 0$, which indicates that the discontinuity at this point moves vertically upward, we choose A, B, C, ... as the interpolation stencil; otherwise, $s_A < 0$, which indicates that the discontinuity at this point moves vertically downward, we choose A, D, E, ... as the interpolation stencil. The vertical critical intervals is treated similarly.

When the stencils are formed for only two points, it is easy to see how this choice of stencils eliminates wiggles and stabilizes the computations. For example, assume that $s_A > 0$ and A deviates a little left from its correct location. This deviation decreases the α and increases the β in (3.18), so that it increases the x speed in (3.13). Thus, A moves faster than expected, and at the following level the wiggle disappears. On the other hand, choosing (A, D) as the stencil will amplify the wiggle.

5. *Handling of Triangles*

The discontinuity curve may intersect a grid cell obliquely so that it cuts out a triangle. An example is displayed in Fig. 3.3, in which the discontinuity curve C cuts out the triangle ΔOAB from a grid cell T. Particular handling of these triangles is described below:

First, when the triangle is very small, the discontinuity positions in the two related horizontal and vertical critical intervals, e.g., A and B in Fig. 3.3, will be very close to each other. Therefore, if we successively choose discontinuity positions for the interpolating stencils in computation of the normal vectors, some stencils will have these two closely neighboring points. This type of stencil may not be good, since these two points together with other points in the stencil may not have a smooth pattern. To avoid this type of stencil, a criterion based on the observation of distances between adjacent positions is set up in choosing points. Thus, when A and B in Fig. 3.3 are too close to each other, we skip B and choose C as the next point in the stencil.

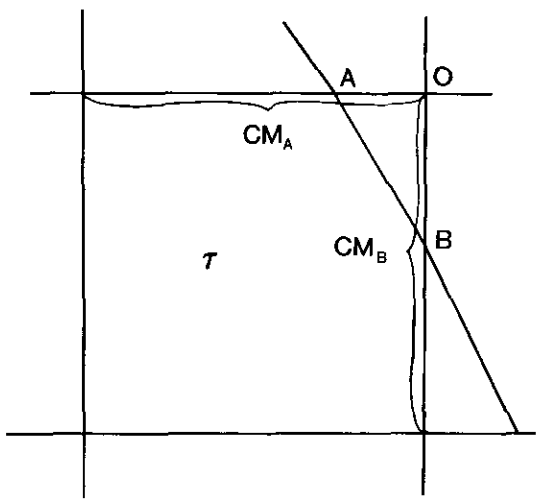

FIG. 3.3. Discontinuity curve C intersects the grid cell T obliquely and forms a triangle OAB. CM_A and CM_B are the horizontal and vertical critical mesh intervals whose movements should match each other.

Second, the movements of the two related horizontal and vertical critical intervals must match each other to keep the continuity of the discontinuity curve. Denote the two related horizontal and vertical critical intervals containing A and B by CM_A and CM_B, respectively. We stipulate that only the following two cases are valid: either both CM_A and CM_B cross over the grid point O to advance to their adjacent intervals, or none of them does. There should be different ways to accomplish it. In this paper we simply stipulate that, if one of the critical intervals advance to the adjacent interval according to its new discontinuity position, the other will do so too, even though its new discontinuity position might be a bit out of its critical interval at the new level. The numerical experiments show that such a little deviation of the discontinuity positions from their corresponding critical intervals does not cause any problems.

When both A and B in Fig. 3.3 cross over O, the numerical solution at O is updated by the mean value of the extrapolated data from the x and y directions, respectively.

6. *Cases of Small α or β*

When one of the components of the normal vectors, i.e., α or β, is very small, which means that the discontinuity curve is almost horizontal or vertical, there are some geometric difficulties that do not occur in the one-dimensional case.

First, the moving speeds evaluated by (3.13) and (3.14) might be very high. Therefore, the discontinuity positions might cross over more than one grid interval along grid lines within one timestep, no matter how the mesh ratio is restricted. Fig. 3.4a gives such an example, in which the horizontal critical interval CM_A moves two grid intervals to the right when the discontinuity curve advances from C^n to C^{n+1} within one timestep.

According to the discussion in the last subsection, if one of CM_A and CM_B advances across O according to its discontinuity position, the other will do so too. Since α is very small, A's new position may have a rather big error; therefore, it is not proper to decide in the same way whether CM_A and CM_C should move across O_1. We stipulate that if CM_C advances across O_1 according to C's new position,

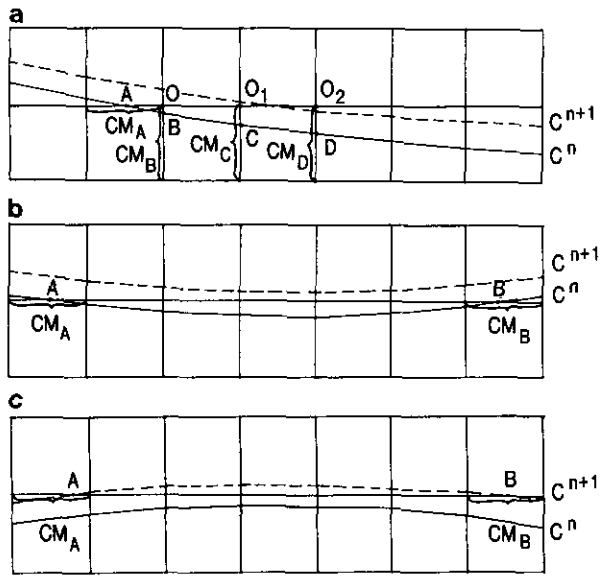

FIG. 3.4. (a) Critical mesh interval CM_A advances two mesh intervals to the right when the discontinuity curve advances from C^n to C^n. (b) Critical mesh intervals CM_A and CM_B are lost when the discontinuity curve advances from C^n to C^{n+1}. (c) Critical mesh intervals CM_A and CM_B are obtained when the discontinuity curve advances from C^n to C^{n+1}. Their discontinuity positions are chosen to be their middle points.

then CM_A will do so too; otherwise, CM_A will not, no matter where A's new position is. In doing so, we let CM_C's movement dominate the situation. The cases for grid points O_2, ... are treated in the same way.

If CM_A crosses O_1, the numerical solution at this point will be updated by the extrapolated data along the y direction. Also an adjustment of A is needed if it deviates too much (say, more than one grid interval) from its critical interval at the new level, since this will cause some problems in computing the normal vectors. In this paper, if A deviates too much from its critical interval, we simply put it back into the critical interval.

Second, the discontinuity may lose critical intervals when it propagates. Figure 3.4b gives such an example, in which the critical intervals CM_A and CM_B are lost when the discontinuity curve moves from C^n to C^{n+1}.

Third, the discontinuity may obtain new critical intervals when it propagates. Figure 3.4c gives such an example, in which the critical intervals CM_A and CM_B are obtained when the discontinuity curve moves from C^n to C^{n+1}. There would be several ways to determine the discontinuity positions for the newly generated citical intervals; however, in this paper we simply choose their middle points as the discontinuity positions.

The adjustment and choice of discontinuity positions described above are not very accurate. Therefore, they may produce wiggles for the discontinuity curve. However, the numerical experiments show that the "upwind" choice of the interpolation stencils described in Subsection 4 will smooth the curve soon afterward.

7. *Implementation of the Treatment for Predictor–Corrector Underlying Scheme*

We implement the treatment in both the predictor and corrector steps. However, only in the predictor steps will the critical intervals move to other intervals. In the corrector steps the critical intervals do not move, no matter where their discontinuity positions are.

For a critical interval, the predictor step gives a discontinuity position $\xi^{n+1/2}$ and the corrector step gives a position $\tilde{\xi}^{n+1}$. The discontinuity position at the following level is finally given by

$$\xi^{n+1} = \tfrac{1}{2}(\xi^n + \tilde{\xi}^{n+1}). \tag{3.20}$$

When a critical interval moves to other grid interval in a predictor step, the numerical solution $u^n_{i,j}$ during the corrector step in (3.2) should be replaced by the extrapolated data from the same side of the discontinuity at the grid point crossed over by the discontinuity curve at level n.

If the forward Euler scheme is second-order accurate in space and the treatment uses the second-order extrapolation, then the numerical solutions and the discontinuity positions are also second-order accurate, provided that the exact solutions to (3.1) are piecewise smooth.

8. *Extension of the Treatment to Euler Equations of Gas Dynamics*

For the Euler equations of gas dynamics in two space dimensions, u, f, and g in (3.1) are

$$\begin{aligned} u &= (\rho, M_x, M_y, E), \\ f(u) &= q_x u + (0, P, 0, q_x P), \\ g(u) &= q_y u + (0, 0, P, q_y P), \end{aligned} \tag{3.21a}$$

where

$$\begin{aligned} &P = (\gamma - 1)(E - \tfrac{1}{2}\rho q^2), \qquad q^2 = q_x^2 + q_y^2, \\ &M_x = \rho q_x, \qquad M_y = \rho q_y, \end{aligned} \tag{3.21b}$$

and

$$c^2 = (\gamma - 1)\left(H - \frac{1}{2}q^2\right), \qquad H = \frac{E+P}{\rho}, \tag{3.21c}$$

where ρ is density, M_x and M_y are x and y momentums, respectively, P is pressure, c is sound speed, and H is enthalpy.

As in the one-dimensional case, we solve the Riemann problems related to the original and extrapolated data to obtain the data that will be used in steps (2), (3), and (4). The Riemann problems are solved along the normal directions at the discontinuity positions. For example, assume

that $[x_{i_1}, x_{i_1+1}]$ is a horizontal critical interval on the grid line $y = y_j$ (see Fig. 3.1). We compute the numerical solution at the grid point $P_2(x_{i_1}, y_j)$. To compute the data that will replace the original data at the point (x_{i_1+1}, y_j) in the numerical fluxes, we solve the Riemann problem related to $u^{n,-}_{i_1+1,j}$ and $u^n_{i_1+1,j}$ along $(\alpha^n_{x,i_1,j}, \beta^n_{x,i_1,j})$. If the discontinuity is a left shock, we pick the original extrapolated data; if it is a right shock, we pick the right middle state; and if it is a contact discontinuity, we pick the left middle state. In doing so, we will not hinder the waves of other types propagating away from the discontinuity.

4. CONSERVATION FEATURE OF THE TREATMENT

In this section, we shall study the conservation feature of the two-dimensional treatment for an isolated discontinuity (scalar case). To do this, we first briefly recall the conservation feature of the one-dimensional treatment discussed in [13]. The one-dimensional treatment is not conservative. This is because the computation uses the extrapolated data on each side of the discontinuities. As a result, different numerical fluxes are used in some grid cells, which harms the conservation. However, we can still write the overall algorithm in a conservation-like form, i.e.,

$$u_j^{n+1} = u_j^n - \lambda(\hat{f}^n_{j+1/2} - \hat{f}^n_{j-1/2}) + p^n_{j+1/2} - p^n_{j-1/2} + q_j^{n+1} - q_j^n, \tag{4.1}$$

where $\hat{f}$ is defined as

$$\hat{f}^n_{j+1/2} = \begin{cases} \hat{f}^{n,-}_{j+1/2}, & j < j_1 \\ \hat{f}^{n,+}_{j+1/2}, & j \geqslant j_1, \end{cases} \tag{4.2}$$

$[x_{j_1}, x_{j_1+1}]$ is the critical cell, the q^n's, which balance the different fluxes used in the same cells, are the local conservation errors, and the p^n's transport the local conservation errors when the discontinuity moves to one of its adjacent cells. Therefore, the p^n's and q^n's are nonzero only in the vicinity of the critical cell. Moreover, the p^n's are nonzero only when the discontinuity moves to a new cell. Instead of u^n, $u^n - q^n$ is conserved in this conservationlike form.

For an isolated discontinuity, the nonzero p^n's and q^n's are given as follows: When ξ^{n+1} remains in the original critical cell $[x_{j_1}, x_{j_1+1}]$,

$$q_{j_1}^{n+1} = q_{j_1}^n + \lambda(\hat{f}^{n,+}_{j_1+1/2} - \hat{f}^{n,-}_{j_1+1/2}); \tag{4.3}$$

when ξ^{n+1} moves to the left adjacent cell,

$$\begin{aligned} p^n_{j_1-1/2} &= -q^n_{j_1} + (u^n_{j_1} - u^{n,+}_{j_1}) \\ &\quad + \lambda(\hat{f}^{n,-}_{j_1-1/2} - \hat{f}^{n,+}_{j_1-1/2}) - R_1, \\ q^{n+1}_{j_1-1} &= -p^n_{j_1-1/2}; \end{aligned} \tag{4.4}$$

and, finally, when ξ^{n+1} moves to the right adjacent cell,

$$\begin{aligned} p^n_{j_1+1/2} &= q^n_{j_1} + \lambda(\hat{f}^{n,+}_{j_1+1/2} - \hat{f}^{n,-}_{j_1+1/2}), \\ q^{n+1}_{j_1+1} &= q^n_{j_1} + (u^{n,-}_{j_1+1} - u^n_{j_1+1}) \\ &\quad + \lambda(\hat{f}^{n,+}_{j_1+3/2} - \hat{f}^{n,-}_{j_1+3/2}) + R_2, \end{aligned} \tag{4.5}$$

where, R_1 and R_2 in (4.4) and (4.5) are now detailed. When the discontinuity crosses over x_{j_1}, we denote by $\bar{u}^{n+1,+}_{j_1}$ the numerical solution computed at this point, using only information from the right side, i.e.,

$$\bar{u}^{n+1,+}_{j_1} = u^{n,+}_{j_1} - \lambda(\hat{f}^{n,+}_{j_1+3/2} - \hat{f}^{n,+}_{j_1+1/2}), \tag{4.6}$$

and $u^{n+1,+}_{j_1}$ the extrapolated datum from the right side at the new level. If $u^{n+1}_{j_1}$ is updated by $\bar{u}^{n+1,+}_{j_1}$, R_1 is zero; otherwise, if it is updated by $u^{n+1,+}_{j_1}$, R_1 is $u^{n+1,+}_{j_1} - \bar{u}^{n+1,+}_{j_1}$. R_2 is obtained similarly. Obviously, when both the underlying scheme and the treatment are the rth-order accurate, R_1 and R_2 are of $O(h^r)$ if they are not zero.

Equations (4.3)–(4.5) describe how the local conservation error for the isolated discontinuity accumulates and compensates the numerical solution. In all the three cases, the flux difference within the cell, which is either $\lambda(\hat{f}^{n,+}_{j_1+1/2} - \hat{f}^{n,-}_{j_1+1/2})$ in (4.3), $\lambda(\hat{f}^{n,+}_{j_1-1/2} - \hat{f}^{n,-}_{j_1-1/2})$ in (4.4), or $\lambda(\hat{f}^{n,+}_{j_1+3/2} - \hat{f}^{n,-}_{j_1+3/2})$ in (4.5), is added to the local conservation error. When the discontinuity crosses over one of the endpoints of the critical cell, $u^n_{j_1} - u^{n,+}_{j_1} - R_1$ or $u^n_{j_1+1} - u^{n,-}_{j_1+1} - R_2$ is deducted from the local conservation error, which is transferred to the numerical solution by updating the solution at nearby grid points.

The Proposition 3.1 in [13] says that if both the underlying scheme and the treatment are first-order accurate, then

$$q^n_{j_1} h = (\xi^n - x_{j_1+1/2})(u^n_{j_1+1} - u^n_{j_1}) + O(h), \tag{7}$$

and if both the underlying scheme and the treatment are second-order accurate, then

$$q^n_{j_1} h = \frac{\begin{pmatrix} (u^n_{j_1} - u^{n,+}_{j_1})(x_{j_1+1} - \xi^n)^2 \\ + (u^n_{j_1+1} - u^{n,-}_{j_1+1})(\xi^n - x_{j_1})^2 \end{pmatrix}}{2h} + O(h^2). \tag{4.8}$$

From this proposition, we see that the local conservation errors are uniformly bounded when the numerical solution is uniformly bounded. This implies that, if the numerical solution with a finite number of isolated discontinuities converges, then it will converge to a weak solution of (2.1).

The proof of (4.8) in [13] is long and complicated. However, the proof of (4.7) is quite simple. It can be completed by showing that (4.7) is exact when the solution is piecewise constant, i.e.,

$$q^n_{j_1} = (\xi^n - x_{j_1+1/2})(u_L - u_R), \tag{4.9}$$

where, u_L and u_R are the solution at the left and right sides of the discontinuity. In fact, in this case the flux difference simply reduces to $\lambda(f(u_R)-f(u_L))$, which is nothing but $(\xi^{n+1}-\xi^n)(u_R-u_L)/h$. When the critical cell moves to the left of right, the deduction from the local conservation error is u_L-u_R or u_R-u_L, respectively. Therefore, the conclusion follows easily.

Now we turn to the conservation feature of the two-dimensional treatment for an isolated discontinuity. For simplicity, we assume that the discontinuity is almost oblique, so that the cases discussed in Section 3.6 will not occur.

Obviously, the overall algorithm can also be written in the conservation-like form

$$\begin{aligned} u_{i,j}^{n+1} = u_{i,j}^n &- \frac{\lambda}{2}(\hat{f}_{i+1/2,j}^n - \hat{f}_{i-1/2,j}^n) \\ &- \frac{\lambda}{2}(\tilde{g}_{i,j+1/2}^n - \tilde{g}_{i,j-1/2}^n) \\ &+ p_{x,i+1/2,j}^n - p_{x,i-1/2,j}^n \\ &+ p_{y,i,j+1/2}^n - p_{y,i,j-1/2}^n \\ &+ q_{x,i,j}^{n+1} - q_{x,i,j}^n + q_{y,i,j}^{n+1} - q_{y,i,j}^n, \end{aligned} \tag{4.10}$$

where the p^n's and q^n's are nonzero only in the vicinity of the critical intervals. The notations are identical as in relation (4.11), where the x and y indexes stand for horizontal and vertical critical intervals.

In (4.10), $\hat{f}$ and $\tilde{g}$ are defined in the same way as $\hat{f}$ in the one-dimensional case. For example, for the isolated discontinuity described in Fig. 3.1, in the vicinity of the horizontal critical interval $[x_{i_1}, x_{i_1+1}]$ on the grid line $y=y_j$,

$$\hat{f}_{i+1/2,j}^n = \begin{cases} \hat{f}_{i+1/2,j}^{n,-} & \text{when} \quad i \leqslant i_1 \\ \hat{f}_{i+1/2,j}^{n,+} & \text{when} \quad i \geqslant i_1+1; \end{cases} \tag{4.11}$$

and in the vicinity of the vertical critical interval $[y_{j_1}, y_{j_1+1}]$ at grid line $x=x_i$,

$$\tilde{g}_{i,j+1/2}^n = \begin{cases} \tilde{g}_{i,j+1/2}^{n,-} & \text{when} \quad j \leqslant j_1 \\ \tilde{g}_{i,j+1/2}^{n,+} & \text{when} \quad j \geqslant j_1+1. \end{cases} \tag{4.12}$$

In this section, we want to show that if we properly choose the p^n's, then the q^n's can also be related to the discontinuity positions. Therefore, if the numerical solution is uniformly bounded, these local conservation errors are uniformly bounded too. Thus implies that, if the numerical solution converges, then it will converge to a weak solution of (3.1).

In the two-dimensional case, different fluxes are also used in some intervals due to the use of extrapolated data. For a critical interval $[x_{i_1}, x_{i_1+1}]$ on the grid line $y=y_j$, if ξ^{n+1} either remains in the original critical interval or advances to the left or right adjacent interval, then the flux difference is either $(\hat{f}_{i_1+1/2,j}^{n,+} - \hat{f}_{i_1+1/2,j}^{n,-})$ or $(\hat{f}_{i_1-1/2,j}^{n,+} - \hat{f}_{i_1-1/2,j}^{n,-})$ or $(\hat{f}_{i_1+3/2,j}^{n,+} - \hat{f}_{i_1+3/2,j}^{n,-})$. Similar results can also be obtained when the critical interval moves across several intervals. The flux difference related to vertical critical intervals is computed similarly.

Just as in the one-dimensional case, the local conservation errors are accumulated by these flux differences. Also, when the discontinuity crosses over grid points, the local conservation errors compensate for the numerical solution to keep the conservation. However, in the two-dimensional case, in order to let the local conservation errors match in the discontinuity positions, the accumulation and compensation should proceed in a particular fashion. The following describes the accumulation and compensation for horizontal critical intervals. The case of vertical critical intervals are similar.

Assume that $[x_{i_1}, x_{i_1+1}]$ is a horizontal critical interval on the grid line $y=y_j$, with normal $(\alpha_{x,i_1,j}^n, \beta_{x,i_1,j}^n)$ at the position $\xi_{x,i_1,j}^n$ (see Fig. 4.1a). The amount of the flux difference that will be added to the $q_{x,i_1,j}^n$ consists of horizontal and vertical parts. The horizontal part is the flux difference related to this critical interval multiplied by $(\alpha_{x,i_1,j}^n)^2$. The

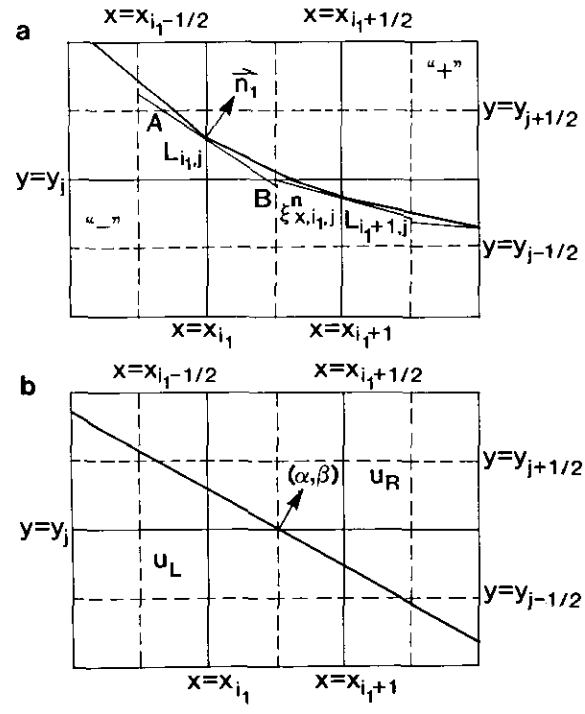

FIG. 4.1. (a) $[x_{i_1}, x_{i_1+1}]$ is a critical mesh interval on the grid line $y=y_j$, with discontinuity position $\xi_{x,i_1,j}^n$ and normal $\mathbf{n}_1=(\alpha_{x,i_1,j}^n, \beta_{x,i_1,j}^n)$. The line segment $L_{i_1,j}$ for the critical mesh interval $[y_j, y_{j+1}]$ on the grid line $x=x_{i_1}$ intersects the strip $y_{j-1/2} \leqslant y \leqslant y_{j+1/2}$ with AB. The line segment $L_{i_1+1,j}$ for the critical mesh interval $[y_{j-1}, y_j]$ on the grid line $x=x_{i_1+1}$ falls entirely into the strip. (b) A straight line discontinuity separates the numerical solution into two parts, namely u_L and u_R.

vertical part consists of the flux differences coming from the nearby vertical critical intervals and is described below:

For a vertical critical interval $[y_j, y_{j+1}]$ at a grid line $x = x_i$, we draw a line segment $L_{i,j}$, which is centered at $\xi^n_{x,i,j}$, located between lines $x = x_{i-1/2}$ and $x = x_{i+1/2}$, and has the normal $(\alpha^n_{x,i,j}, \beta^n_{x,i,j})$. If $L_{i,j}$ intersects the strip $y_{j-1/2} \leqslant y \leqslant y_{j+1/2}$, we denote by R the ratio of the lengths of the part that falls into the strip and $L_{i,j}$ itself. For example, since the line segment $L_{i_1,j}$ for the vertical critical interval $[y_j, y_{j+1}]$ on the grid line $x = x_{i_1}$ intersects the strip with the segment AB (see Fig. 4.1a), R is equal to $|AB|/|L_{i,j}|$. For another example, since the whole line segment $L_{i_1+1,j}$ falls into the strip, R is equal to 1. Then the flux difference related to this vertical critical interval multiplied by $R(\alpha^n_{x,i,j})^2$ goes to the vertical part mentioned above.

The compensations of the local conservation errors to the numerical solution are described as follows: Assume that the discontinuity position crosses over the grid point $[x_{i_1+1}, y_j]$, then it is easy to verify that the deduction of the local conservation errors at this point is

$$u^{n,-}_{i_1+1,j} - u^n_{i_1+1,j} + R_1, \tag{4.13}$$

where $u^{n,-}_{i_1+1,j}$ is the mean value of the extrapolated data from the x and y directions at the level n, and R_1 is as follows: If $u^{n+1}_{i_1+1,j}$ is updated by $\bar{u}^{n+1,-}_{i_1+1,j}$, R_1 is zero; otherwise, if it is updated by $u^{n+1,-}_{i_1+1,j}$;

$$R_1 = u^{n+1,-}_{i_1+1,j} - \bar{u}^{n+1,-}_{i_1+1,j}, \tag{4.14}$$

where $\bar{u}^{n+1,-}_{i_1+1,j}$ is the numerical solution computed using only information from the "$-$" side and $u^{n+1,-}_{i_1+1,j}$ is the mean value of the extrapolated data at the new level. This deduction is shared by $q^n_{x,i_1,j}$ and $q^n_{y,i_1+1,j-1}$. We let $(\alpha^n_{x,i_1,j})^2/((\alpha^n_{x,i_1,j})^2 + (\beta^n_{y,i_1+1,j-1})^2)$ of it go to $q^n_{x,i_1,j}$, and the remaining part is added to $q^n_{y,i_1+1,j-1}$.

Obviously, these accumulations and compensations can be realized by properly choosing the p^n_x and p^n_y.

We show the following relations between the local conservation errors and the discontinuity positions,

$$q^n_{x,i,j}h = (\alpha^n_{x,i,j})^2 (\xi^n_x - x_{i+1/2}) \times (u^n_{i+1,j} - u^n_{i,j}) + O(h) \tag{4.15}$$

for a horizontal critical interval $[x_{i+1}, x_i]$, and

$$q^n_{y,i,j}h = (\beta^n_{y,i,j})^2 (\xi^n_y - y_{j+1/2}) \times (u^n_{i,j+1} - u^n_{i,j}) + O(h) \tag{4.16}$$

for a vertical critical interval $[y_{j+1}, y_j]$. Indeed, (4.15) and (4.16) are the extension of (4.7) in two space dimensions. To do this, we show that for a piecewise constant solution with straight line discontinuities, (4.15) and (4.16) are exact. This implies that they are first-order accurate, in general.

Assume that the normal to the straight line discontinuity is (α, β), and on each side of the discontinuity the solution is u_L and u_R (as shown in Fig. 4.1b). In this case, it is easy to verify that for each horizontal critical interval, the horizontal part of the difference added to the local conservation error is $\alpha^2\lambda(f(u_R) - f(u_L))$, and the vertical part is $\alpha\beta\lambda(g(u_R) - g(u_L))$. Therefore, the total amount of the flux difference added to the local conservation error is

$$\alpha^2\lambda(f(u_R) - f(u_L)) + \alpha\beta\lambda(g(u_R) - g(u_L)). \tag{4.17}$$

When the discontinuity crosses over the left endpoint of the critical interval, the compensation from the local conservation error reduces to $\alpha^2(u_L - u_R)$, and when the discontinuity crosses over the right endpoint, the deduction is $\alpha^2(u_R - u_L)$. The conclusion follows easily from (3.13). The conclusion for a vertical critical interval can follow in the same way.

5. TREATMENT FOR INTERACTIONS OF DISCONTINUITIES IN THE SCALAR CASE

The one-dimension treatment for critical cells that are close to each other, and the "stacking treatment" that deals with the critical cells stacking in the same cell, developed in [13, 14], can be naively extended to the two-dimensional case; therefore, in this section we only focus on the treatment of the triple points where three discontinuities meet.

For simplicity, we only study the scalar case. Our treatment is based on the solution of the following problem: Suppose that three discontinuities L_1, L_2, and L_3 meeting at the trip point, say O, are straight lines. They divide the solution of (3.1) into three constant parts u_1, u_2, and u_3 (as shown in Fig. 5.1). Suppose now that, given L_1 and L_2, we want to determine L_3. Without losing generality we suppose that O is the origin of the (x, y)-plane. Since L_1 separates u_2 and u_3, its normal propagating speed is

$$S_1 = \frac{\alpha_1[f]_{2,3} + \beta_1[g]_{2,3}}{[u]_{2,3}}, \tag{5.1}$$

where (α_1, β_1) is the unit normal vector of L_1, $[f]_{2,3}$ and $[g]_{2,3}$ are the jumps of the two fluxes across L_1, and $[u]_{2,3}$ is the jump of the solution across L_1. Hence, the equation for L_1 is

$$\alpha_1 x + \beta_1 y = S_1 t, \tag{5.2}$$

the equation for L_2 is

$$\alpha_2 x + \beta_2 y = S_2 t, \tag{5.3}$$

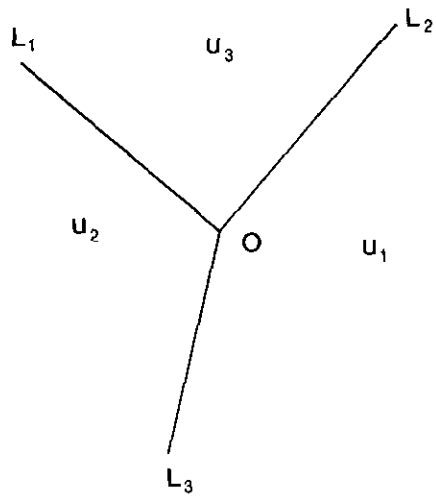

FIG. 5.1. Three straight line discontinuities L_1, L_2, and L_3 meet at point O, separating three constant states u_1, u_2, and u_3. O is the triple point.

where

$$S_2 = \frac{\alpha_2[f]_{3,1} + \beta_2[g]_{3,1}}{[u]_{3,1}}, \tag{5.4}$$

and the equation for L_3 should be

$$\alpha_3 x + \beta_3 y = S_3 t, \tag{5.5}$$

where

$$S_3 = \frac{\alpha_3[f]_{2,1} + \beta_3[g]_{2,1}}{[u]_{2,1}} \tag{5.6}$$

and (α_3, β_3) is the unit normal vector of L_3 to be solved. Because the straight lines L_1, L_2, and L_3 meet at the same point O, the determinant

$$\begin{vmatrix} \alpha_1 & \beta_1 & S_1 \\ \alpha_2 & \beta_2 & S_2 \\ \alpha_3 & \beta_3 & S_3 \end{vmatrix} = 0, \tag{5.7}$$

from which and the restriction $\alpha_3^2 + \beta_3^2 = 1$, α_3 and β_3 can be computed. Particularly, when (α_1, β_1) and (α_2, β_2) are not parallel to each other, there exists k_1 and k_2 so that

$$\begin{aligned} k_1\alpha_1 + k_2\alpha_2 &= \alpha_3 \\ k_1\beta_1 + k_2\beta_2 &= \beta_3 \\ k_1 S_1 + k_2 S_2 &= S_3. \end{aligned} \tag{5.8}$$

Now we are going to build up the treatment of interactions of discontinuities. We call the grid cell that contains the triple point a node. The node should have three critical intervals locating in its four grid intervals, which are related to the three discontinuities. Two of the critical intervals might stack in the same interval.

Figure 5.2 gives two typical cases of the propagation of nodes. In Fig. 5.2a, the horizontal critical intervals CM_1 and CM_2 related to discontinuity L_1 and L_2 merge together because their discontinuity positions cross over each other and generate a new critical interval for L_3. In this case, the node advances from the cell M_1 to M_2. In Fig. 5.2b, a vertical critical interval CM_1 related to L_1 advances one interval to the top; hence, the discontinuity L_2 loses its critical interval CM_2, which becomes a new critical interval related to L_3. In this case, the node moves from the cell M_1 to M_2. If we stipulate that only one of the three critical intervals of the node could advance to its adjacent intervals in each timestep, then more general cases can always be reduced to one of the above cases.

The main point of the treatment for the two above cases is to calculate the new discontinuity positions of L_3 by assuming that L_1, L_2, and L_3 are straight lines. Obviously, the treatment will only be first-order accurate since we assume that the discontinuities are straight lines and the solution is piecewise constant near triple points. However, when the solution is piecewise smooth and since the

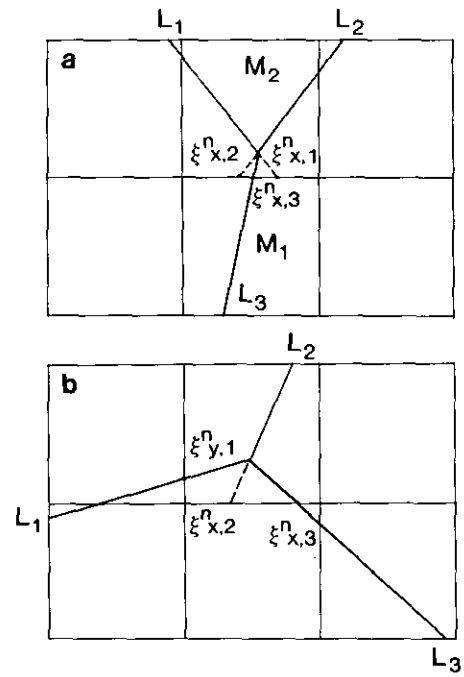

FIG. 5.2. (a) Two horizontal critical mesh intervals CM_A and CM_B related to L_1 and L_2 merge to generate a new critical mesh interval related to L_3. Meanwhile the node advances from cell M_1 to M_2. (b) Vertical critical mesh interval CM_1 related to L_1 advances one mesh interval to the top; hence L_2 loses its critical mesh interval CM_2, which becomes a critical mesh interval related to L_3. Meanwhile the node advances from cell M_1 to M_2.

discontinuity interactions only happen at a rate of $O(h^2)$, the overall algorithm is still second-order accurate.

Now we begin to discuss the case displayed in Fig. 5.2a. Denote by $\xi^n_{x,1}$ and $\xi^n_{x,2}$ the discontinuity positions of the critical intervals CM_1 and CM_2, which cross over each other, by $\xi^n_{x,3}$, the discontinuity position of the newly generated critical interval, and by (x_O, y_O), the coordinates of the triple point O. Since L_1, whose normal is (α_1, β_1), passes through O, $\xi^n_{x,1}$, which lies on L_1, satisfies

$$\alpha_1(\xi^n_{x,1} - x_O) + \beta_1(y_{j_1} - y_O) = 0, \tag{5.9}$$

where y_{j_1} is the y-coordinate of the left end point of the critical interval. By the same argument,

$$\alpha_2(\xi^n_{x,2} - x_O) + \beta_2(y_{j_1} - y_O) = 0 \tag{5.10}$$

and

$$\alpha_3(\xi^n_{x,3} - x_O) + \beta_3(y_{j_1} - y_O) = 0. \tag{5.11}$$

Multiplying (5.9) and (5.10) by k_1 and k_2 defined in (5.8), summing them, subtracting (5.11) and using (5.8), we obtain

$$\xi^n_{x,3} = \frac{k_1\alpha_1\xi^n_{x,1} + k_2\alpha_2\xi^n_{x,2}}{\alpha_3}, \tag{5.12}$$

which is the formula to calculate $\xi^n_{x,3}$.

For the case shown in Fig. 5.2b, we denote by $\xi^n_{y,1}$ the discontinuity position of CM_1. By a similar argument, we have

$$\alpha_1(x_{i_1} - x_O) + \beta_1(\xi^n_{y,1} - y_O) = 0 \tag{5.13}$$

and (5.9) and (5.10), from which we obtain

$$\xi^n_{x,3} = \frac{k_1(\alpha_1 x_{i_1} + \beta_1(\xi^n_{y,1} - y_{j_1})) + k_2\alpha_2\xi^n_{x,2}}{\alpha_3}. \tag{5.14}$$

The treatment also has a conservation feature in some weak sense; however, its discussion will be quite complicated and a forthcoming paper will mainly focus on it.

6. PROGRAMMING OF THE ALGORITHM

Although the algorithm is a front tracking method, its programming is not as complicated as thought to be. In fact, it could be programmed in a shock capturing fashion with little knowledge of the geometry of the tracked discontinuities. This is possible because of the following two reasons:

(1) The method tracks the discontinuity along grid lines rather than its normal direction, so that the computation has been mainly kept on the regular grid.

(2) The method does not have flow states at the tracked discontinuity, so that there is no CFL-restriction on the timestep caused by the calculation of these states.

The data structure for the tracked discontinuity are "critical intervals," which contain the discontinuity positions, the normals to the discontinuity at this position, the type of the discontinuity, and the addresses of two geometric and two physical neighboring critical intervals. The two geometric neighboring critical intervals are the two adjacent critical intervals related to the same discontinuity, and the two physical neighboring critical intervals are the nearest left and right critical intervals on the same grid line. The geometric neighbor relation is required in computing the normal to the discontinuity, and the physical neighbor relation is required when dealing with the critical intervals that are close to each other or stack in the same interval.

The data structure for the discontinuity interaction point are "nodes" which contain the addresses of the three critical intervals on its edges. These critical intervals only have one geometric neighboring critical interval, and their stencils for computing the normals are picked from one side only.

The algorithm was programmed in FORTRAN 77; however, the author recently learned from [2, 7] that C could be a better language to deal with these types of data structures, because its utilities *pointer* and *record* can effectively handle them.

The computation is implemented as follows: In each predictor or corrector step of the algorithm, we first compute the numerical solution without considering the critical

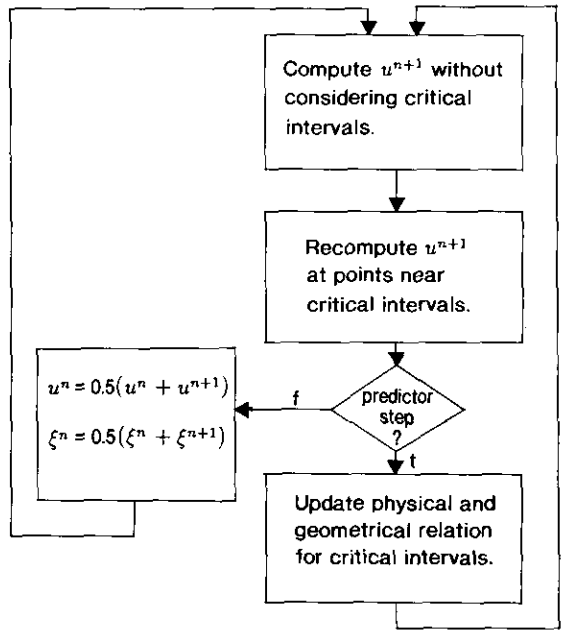

FIG. 6.1. The flow chart of the algorithm.

intervals. Then we recompute the numerical solution at the points near critical intervals. In the predictor step, we should update the critical intervals and nodes and their geometric and physical relations according to the new discontinuity positions. Denote by u the numerical solution and by ξ the discontinuity position; Fig. 6.1 is the flow chart of the program.

7. NUMERICAL EXPERIMENTS

In this section we shall display four numerical examples computed by using the treatment to track the discontinuities. The numerical fluxes used in the underlying scheme (3.2) for both f and g are the second-order TVD flux described in [17].

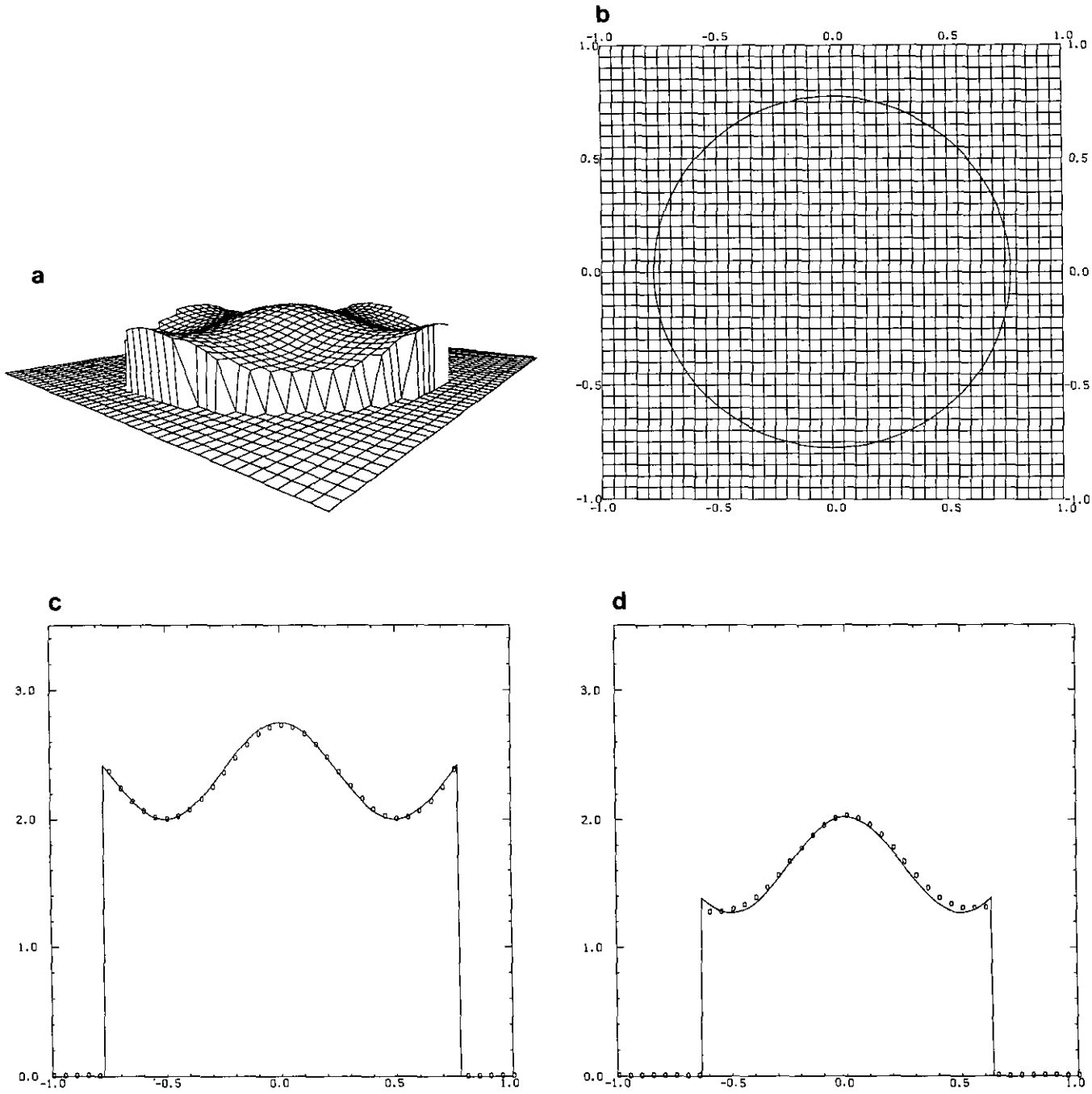

FIG. 7.1. (a) Surface, $t = 2.0$ (160 steps); (b) location of discontinuity, $t = 2.0$ (160 steps); (c) $x = 0.0$, $t = 2.0$ (160 steps); (d) $y = 0.45$, $t = 2.0$ (160 steps).

EXAMPLE 1. This is an example for the linear case. The partial differential equation is

$$u_t + u_x + u_y = 0, \qquad |x| \leqslant 1, \ |y| \leqslant 1, \tag{7.1}$$

with initial data

$$u(x, y, 0) = u_0(x, y) = \begin{cases} 0.75 \cos((x+y)\pi)\cos((x-y)\pi), \\ \qquad x^2 + y^2 \leqslant 0.6 \\ 0, \qquad \text{otherwise} \end{cases} \tag{7.2}$$

and periodic boundary conditions. The exact solution of this problem is

$$u(x, y, t) = u_0(x - t, y - t), \tag{7.3}$$

which has a discontinuity circle with radius $\sqrt{6}$. The mesh ratio is chosen to be 0.5 and $\Delta x = \Delta y = 0.05$. Figure 7.1a shows the numerical solution at $t = 2$ (160 timesteps). Figure 7.1b shows the discontinuity circle of the numerical

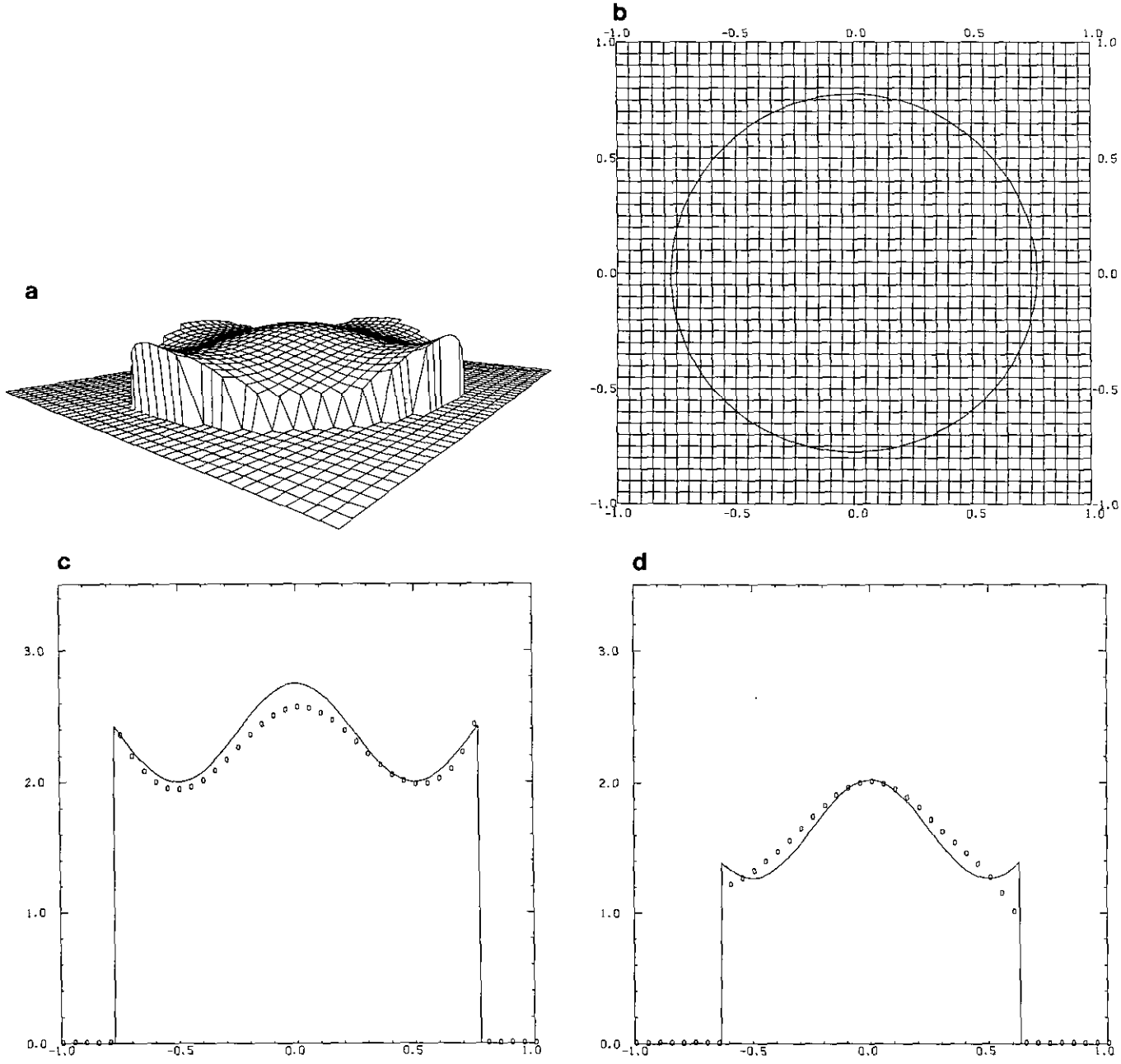

FIG. 7.2. (a) Surface, $t = 16.0$ (1280 steps); (b) location of discontinuity, $t = 16.0$ (1280 steps); (c) $x = 0.0$, $t = 16.0$ (1280 steps); (d) $y = 0.45$, $t = 16.0$ (1280 steps).

solution, which is plotted by connecting the discontinuity positions with line segments. Figures 7.1c and d show the intersection surfaces of the numerical solution at $x = 0$ and $y = 0.45$, respectively, in which the circles represent the numerical solution, and the solid lines represent the exact solution. Figure 7.2 visualizes the solution at time $t = 16$ (1280 timesteps). We can see in the figures that both the numerical solution and the discontinuity positions approximate the exact solution quite well.

EXAMPLE 2. The partial differential for this example is

$$u_t + u_x + u_y = -\mu u(u-1)(u-\tfrac{1}{2}), \tag{7.4}$$

which is a linear advection equation with a stiff source term when μ is large. This equation is interesting since it models reacting flows. Many difference methods would produce wrong propagating speed if its solution has a propagating discontinuity (see [12]). Chang (see [1]) has used the subcell resolution proposed by Harten (see [10]) to the one-dimensional version of this problem and obtained very good numerical results. Here, we use our treatment, which is similar in some sense to Harten's subcell technique (see [14] for relevant discussion), to track the two-dimensional propagating discontinuity.

The initial data is still (7.2), which indicates that the solution has the same propagating discontinuity curve as in the previous example; λ, Δx, and Δy are chosen as before. A Strang-type splitting method suggested in [12] is used to solve this problem, in which the same numerical solution operator with our treatment solves the convection equation without the source term, and an implicit predictor–corrector method for ordinary differential equations models the chemistry. Figure 7.3a shows the numerical solution for $\mu = 0.15$ (non-stiff) at time $t = 1$, and Fig. 7.3b shows the discontinuity circle at the same time. Figures 7.4 visualize the solution when $\mu = 150$ (stiff). In the plots we see that the numerical solutions for both stiff and non-stiff cases have correct propagating speeds.

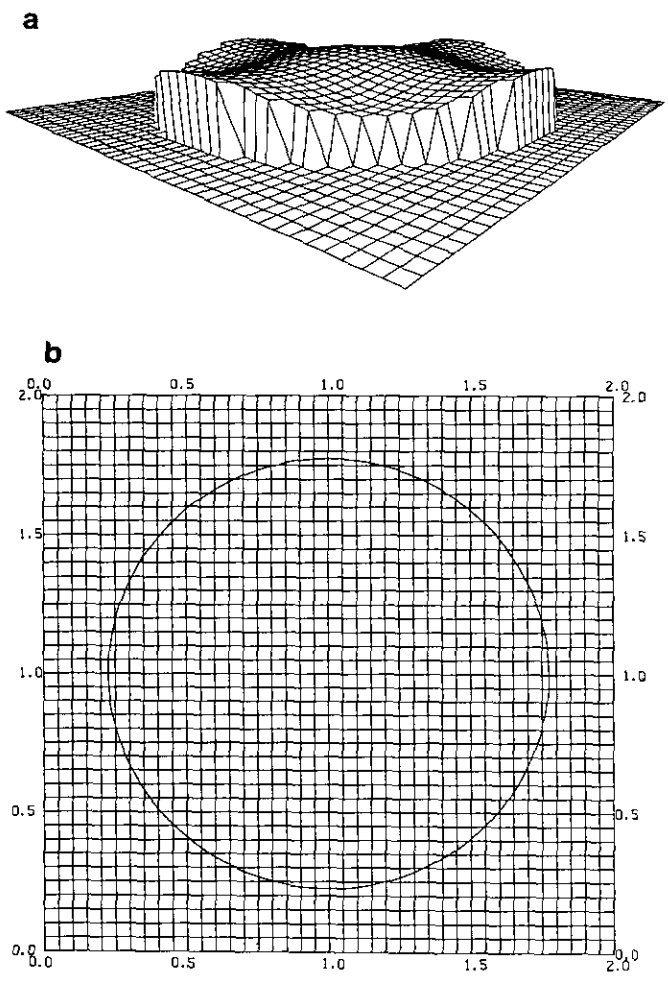

FIG. 7.3. (a) Surface, $t = 1.0$ ($\mu = 0.15$); (b) location of discontinuity, $t = 1.0$ ($\mu = 0.15$).

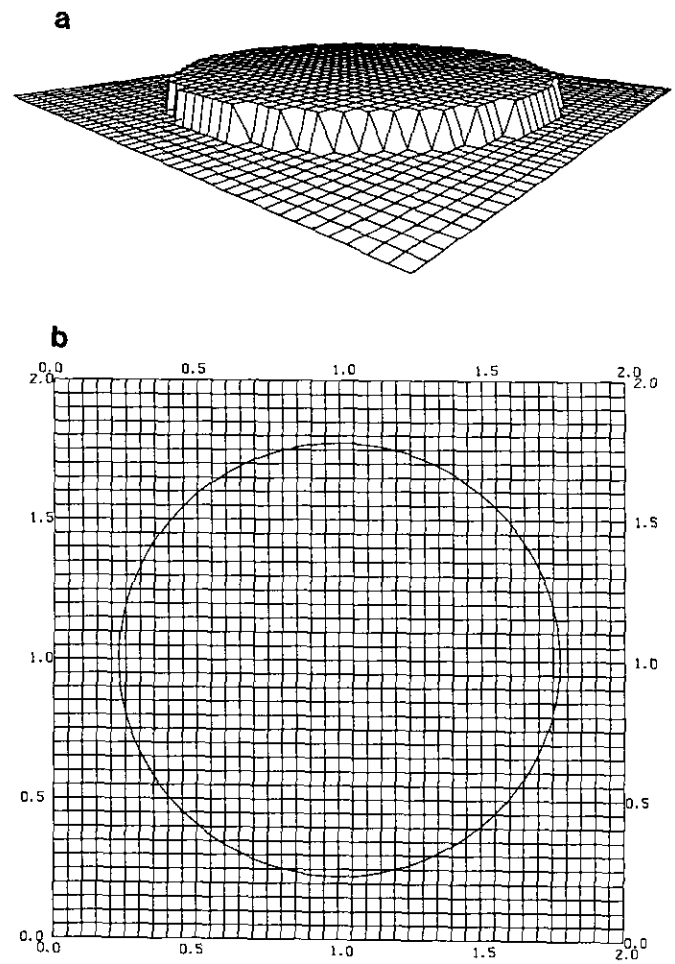

FIG. 7.4. (a) Surface, $t = 1.0$ ($\mu = 150.0$); (b) location of discontinuity, $t = 1.0$ ($\mu = 150.0$).

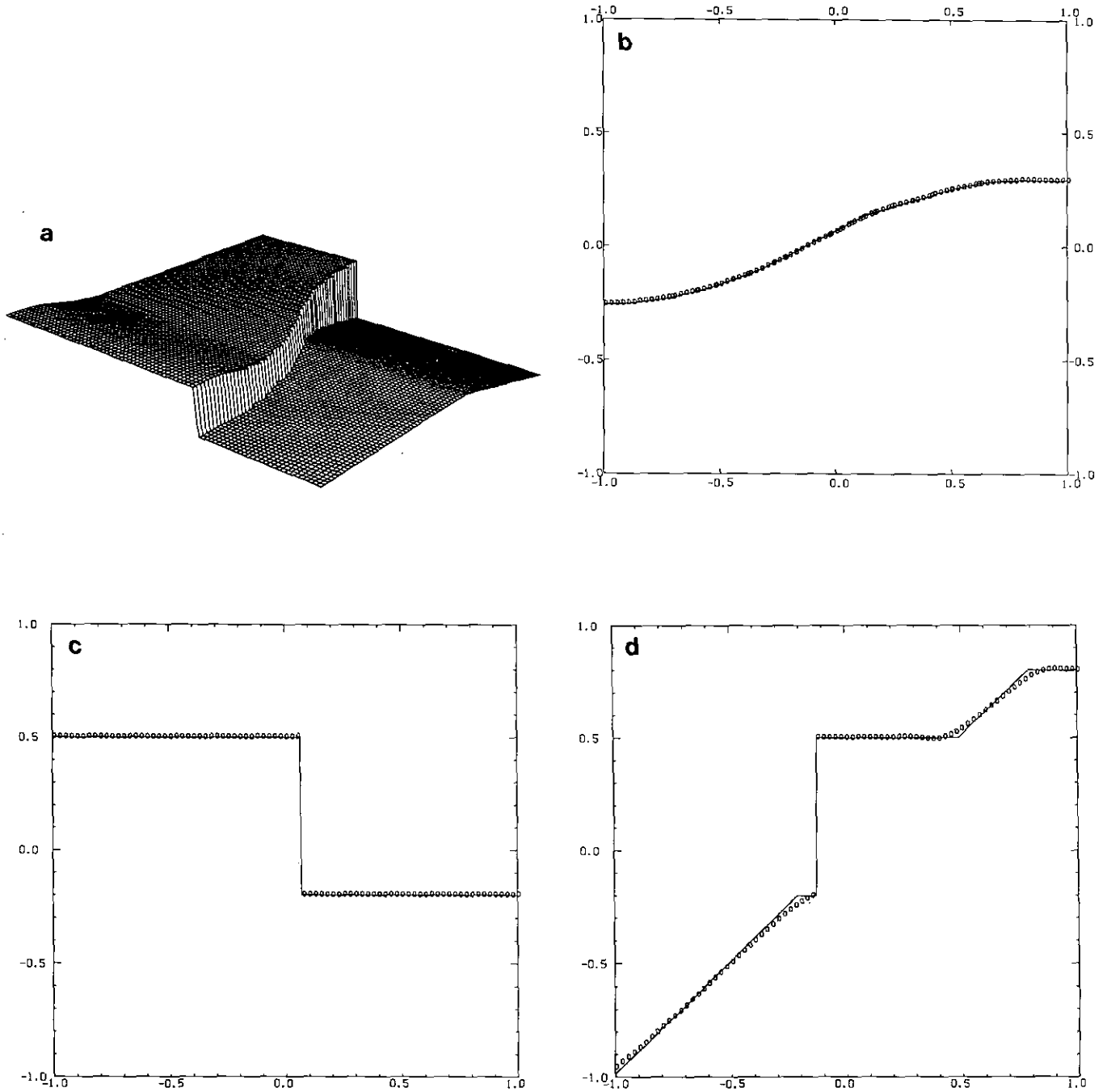

FIG. 7.5. (a) Surface, $t = 1.0$ (160 steps); (b) location of discontinuity, $t = 1.0$ (160 steps); (c) $x = 0.0$, $t = 1.0$ (160 steps); (d) $y = 0.0$, $t = 1.0$ (160 steps).

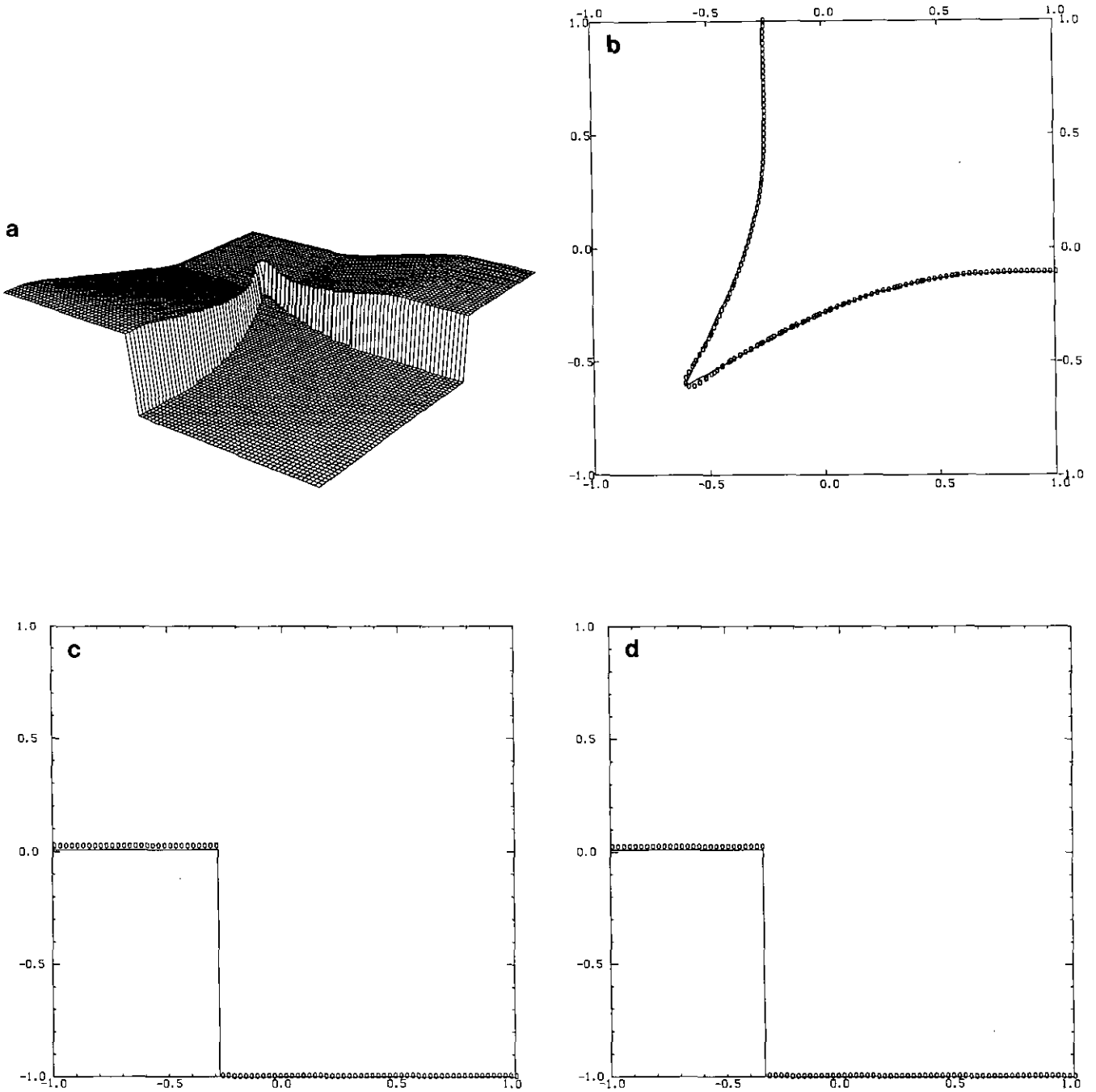

FIG. 7.6. (a) Surface, $t = 1.0$ (160 steps); (b) location of discontinuity, $t = 1.0$ (160 steps); (c) $x = 0.0$, $t = 1.0$ (160 steps); (d) $y = 0.0$, $t = 1.0$ (160 steps).

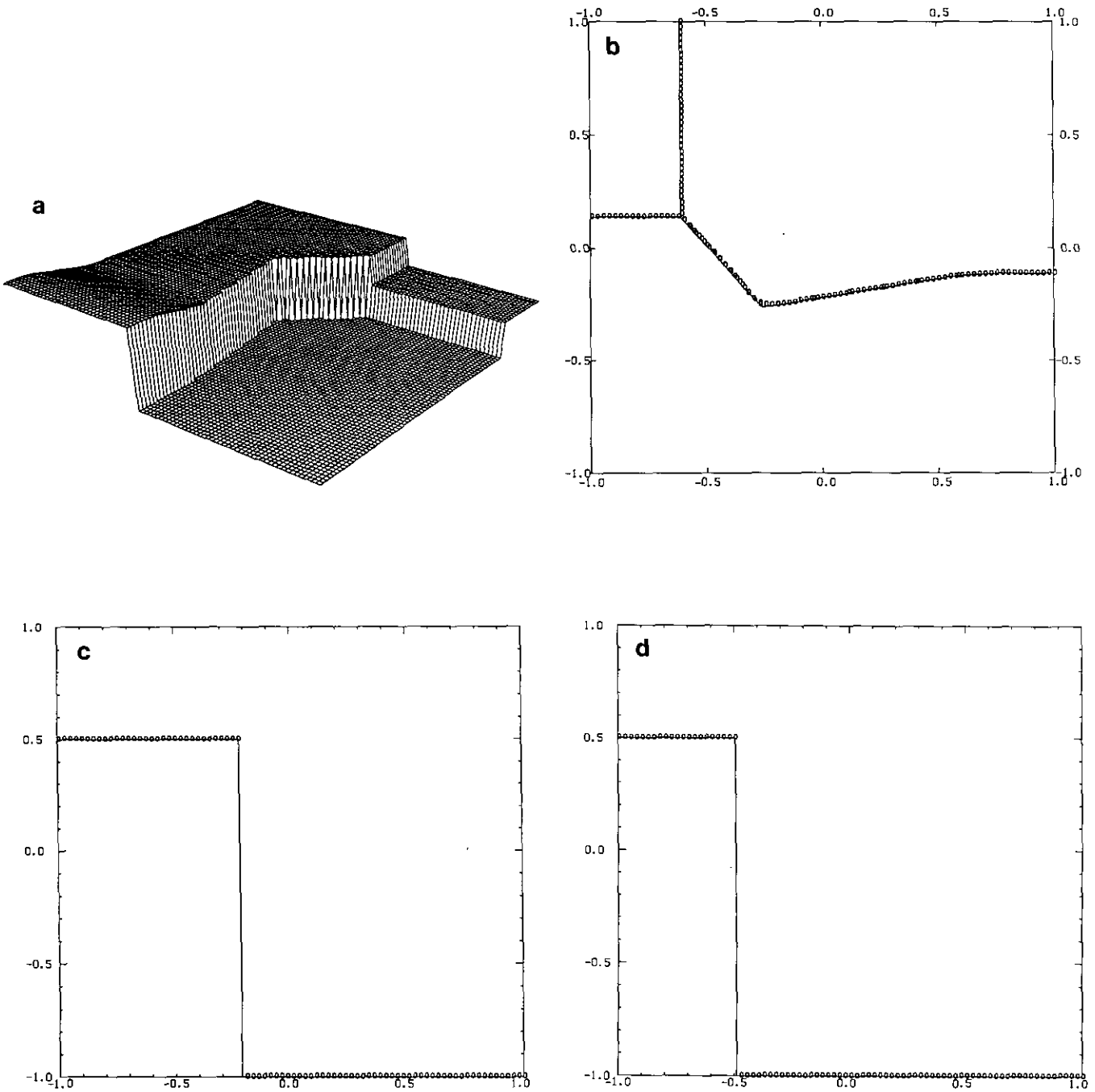

FIG. 7.7. (a) Surface, $t = 1.0$ (160 steps); (b) location of discontinuity, $t = 1.0$ (160 steps); (c) $x = 0.0$, $t = 1.0$ (160 steps); (d) $y = 0.0$, $t = 1.0$ (160 steps).

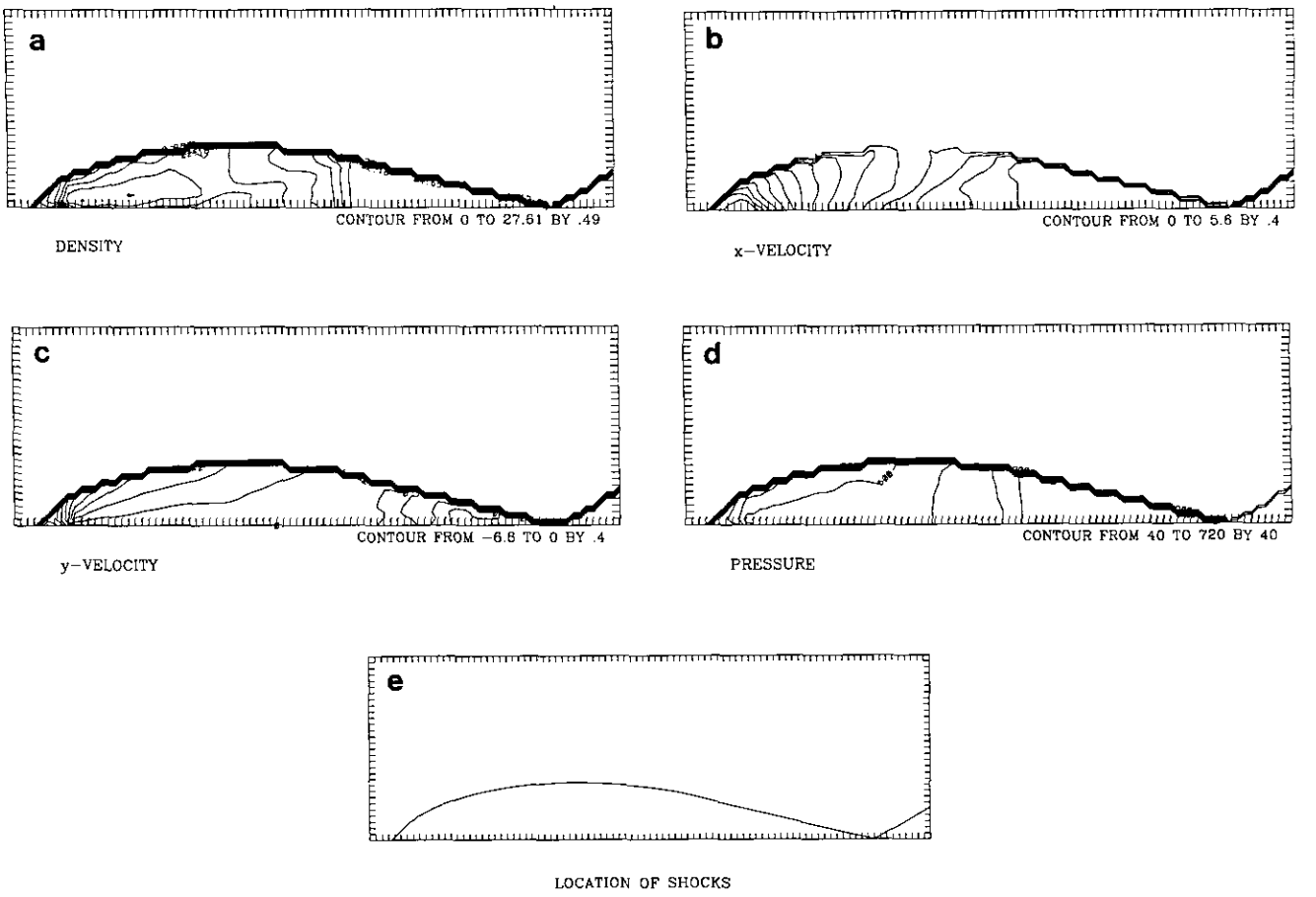

FIG. 7.8. Flow at time 0.12 computed on a grid with $\Delta x = \Delta y = \frac{1}{30}$: (a) density; (b) x-velocity; (c) y-velocity; (d) pressure; (e) is the discontinuity curve.

EXAMPLE 3. This is an example for the nonlinear case. The partial differential equation is

$$u_t + (\tfrac{1}{2}u^2)_x + (\tfrac{1}{2}u^2)_y = 0, \tag{7.5}$$

with the Riemann initial data,

$$u(x, y, 0) = u_0(x, y) = \begin{cases} u_1, & x > 0,\ y > 0, \\ u_2, & x \leqslant 0,\ y > 0, \\ u_3, & x \leqslant 0,\ y \leqslant 0, \\ u_4, & x > 0,\ y \leqslant 0. \end{cases} \tag{7.6}$$

The following three cases are tested:

Case 1,

$$(u_1, u_2, u_3, u_4) = (-0.2, -1.0, 0.5, 0.8).$$

Case 2,

$$(u_1, u_2, u_3, u_4) = (-1.0, 0.5, -0.2, 0.8).$$

Case 3,

$$(u_1, u_2, u_3, u_4) = (-1.0, -0.2, 0.5, 0.8).$$

λ is still chosen to be 0.5 and Δx and Δy are chosen to be 0.025. Figures 7.5, 7.6, and 7.7 show the numerical results at time $t = 1$ in Case 1, Case 2, and Case 3, respectively. All the plots labeled with "a" show the numerical solutions; all the plots labeled with "b" show the discontinuity positions of the numerical solutions, in which the circles represent the numerical positions and the solid lines represent the exact discontinuity curves; and all the plots labeled with "c" and "d" show the intersection surfaces of the numerical solution at $x = 0$ and $y = 0$, respectively. In these figures, we can see that both the numerical solutions and the discontinuity positions approximate the exact ones very well.

The discontinuity curve in Case 2 has a very sharp corner; however, Fig. 7.6b shows that the computation of the discontinuity positions around this corner is stable and still has a reasonable resolution. Case 3 has a triple point formed in the interaction of discontinuities. The treatment for interactions is applied around and the result is quite good.

EXAMPLE 4. This example is a regular shock reflection of the Euler equations of gas dynamics. A planar shock

wave drives down a tube and meets the reflecting wall of the tube with a small angle. When the wall begins to slope, a regular shock reflection occurs which develops a self-similar flow. The example involves a Mach 10 shock in the air ($\gamma = 1.4$), which initially makes a 30° angle with the reflecting wall.

The reflecting wall lies along the bottom of the problem, beginning at $x = \frac{3}{10}$. The shock makes a 30° angle with the x axis and extends to the top of the domain at $y = 1$. The short region from $x = 0$ to $x = \frac{3}{10}$ along the bottom boundary at $y = 0$ is always assigned values for the initial post-shock flow. This boundary condition forces the reflecting shock to be "attached" to the reflecting wall. The left-hand boundary is also assigned values for the initial post-shock flow, and the right-hand and top boundaries are set to describe the exact motion of the initial Mach 10 shock.

We track the incident shock as well as the reflected shock. The reflecting point is treated as a boundary point. The two-dimensional Riemann problem related to this regular reflection is solved to find the data that updates the numerical solution at the boundary grid points crossed over by the shock. At the initial level, a bubble with the size about $\frac{1}{10000}$ of the grid cell in area is set for the region enclosed by the reflected shock around the boundary grid point $x = \frac{3}{10}$. The numerical experiments show that the result is insensitive to the shape of the bubble.

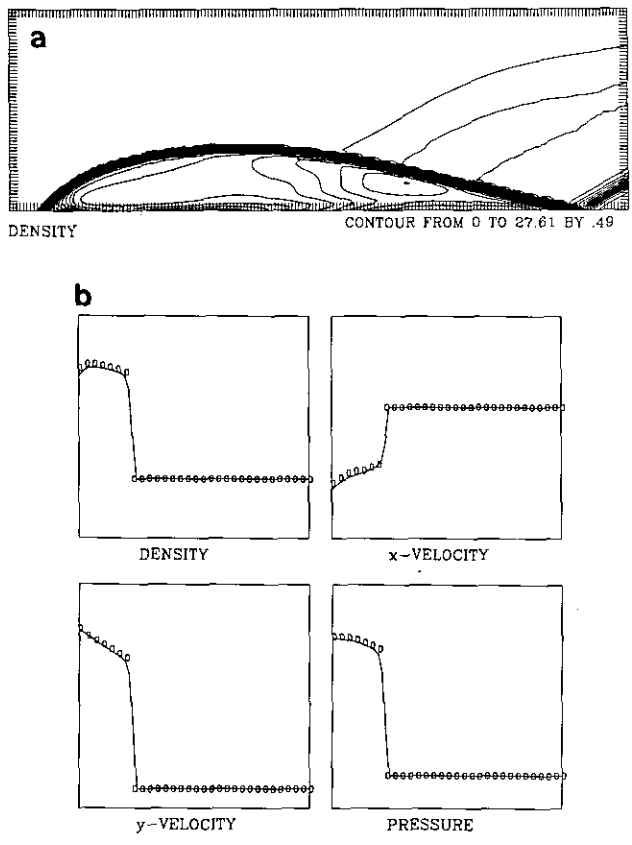

FIG. 7.9. Flow time 0.12 computed on a grid with $\Delta x = \Delta y = \frac{1}{60}$: (a) density; (b) comparison between the numerical solutions with and without the treatment at $x = 0.5$.

The flow at time 0.12, computed on a grid with $\Delta x = \Delta y = \frac{1}{30}$, is displayed in Fig. 7.8, in which the plots a, b, c, and d are the density, x-velocity, y-velocity, and pressure, respectively, and Fig. 7.8e displays the discontinuity curve. The discontinuity displayed in Figs. 7.8a to d has wiggles, because the contour package represents the solution in the critical intervals still as a smooth function.

To validate the method, we also display the numerical result at the same time, computed on a grid with $\Delta x = \Delta y = \frac{1}{60}$, and without the treatment, in Fig. 7.9. Figure 7.9a is the density and Fig. 7.9b displays the comparison between the numerical solutions with and without the treatment at the intersection $x = 0.5$, where the circles and the solid lines are the solution with and without the treatment, respectively. This figure shows excellent agreement of both numerical solutions.

8. CONCLUSIONS

We have built up a treatment for discontinuities for the two-dimensional conservation laws, which extends the one-dimensional treatment introduced in [13]. We also have studied the conservation feature of the treatment for an isolated discontinuity. To do this, we wrote the overall algorithm in a conservation-like form involving local conservation errors and showed that the local conservation errors are uniformly bounded. Treatment for interactions of discontinuities has been also set up; however, the study of its conservation feature is still under investigation. Numerical experiments show that the treatment is a very effective tracking technique.

ACKNOWLEDGMENTS

The author thanks Professor Ami Harten and Stanley Osher, and Dr. Frederic Lafon for helpful discussions and/or English corrections.

REFERENCES

1. S. H. Chang, NASA TM-102384, 1989 (unpublished).
2. I.-L., Chern, J. Glimm, O. McBryan, B. Plohr, and S. Yaniv, *J. Comput. Phys.* **62**, 83 (1986).
3. J. Glimm, J. Grove, B. Lindquist, O. McBryan, and G. Tryggvason, *SIAM J. Sci. Statist. Comput.* **9**, 61 (1988).
4. J. Glimm, *Commun. Pure. Appl. Math.* **41**, 569 (1988).
5. J. Glimm, O. McBryan, R. Menikoff, and H. Sharp, *SIAM J. Sci. Statist. Comput.* **7**, 280 (1986).
6. J. Glimm, C. Klingenberg, O. McBryan, B. Plohr, D. Sharp, and S. Yaniv, *Adv. Appl. Math.* **6**, 259 (1985).
7. J. Glimm and O. McBryan, *Adv. Appl. Math.* **6**, 422 (1985).

8. J. Glimm, E. Isaacson, D. McBryan, and O. McBryan, *Adv. Appl. Math.* **2**, 91 (1981).
9. J. Grove, *Adv. Appl. Math.* **10**, 201 (1989).
10. A. Harten, *J. Comput. Phys.* **83**, 148 (1989).
11. W. D. Henshaw, *J. Comput. Phys.* **68**, 25 (1987).
12. R. J. LeVeque and H. C. Yee, NASA TM-100075, 1988 (unpublished).
13. D. Mao, UCLA CAM Report 90-19, 1990 (unpublished).
14. D. Mao, *J. Comput. Phys.* **92**, 422 (1991).
15. D. Mao, *J. Comput. Math.* **3**, 256 (1985) [Chinese].
16. G. Moretti, Report No. PIBAL-72-37, Polytechnic Institute of Brooklyn, 1972 (unpublished).
17. S. Osher and S. Chakravarthy, ICASE Report 84.44, 1984, IMA Volume in Mathematics and its Applications, Vol. 2, p. 229 (Springer-Verlag, New York/Berlin, 1986).
18. S. Osher and S. Chakravarthy, *SIAM Numer. Anal.* **21**, 955 (1984).
19. S. Osher, *SIAM Numer. Anal.* **21**, 217 (1984).
20. R. Richtmyer and K. Morton, *Difference Methods for Initial Value Problems* (Interscience, New York, 1967).
21. C.-W. Shu, *Math. Comput.* **49**, 105 (1987).
22. B. Swartz and B. Wendroff, *Appl. Numer. Math.* **2**, 385 (1986).
23. D. H. Wagner, *SIAM J. Math. Anal.* **14**, 3 (1983).

JOURNAL OF COMPUTATIONAL PHYSICS 104, 398–417 (1993)

A Discrete Model for MHD Incorporating the Hall Term

F. KAZEMINEZHAD

Physics Department, University of California, Los Angeles

J. N. LEBOEUF

Oakridge National Laboratory, Oakridge, Tennessee

F. BRUNEL

National Research Council of Canada, Montreal, Canada

AND

J. M. DAWSON

Physics Department, University of California, Los Angeles

Received March 30, 1990; revised April 28, 1992

Medium frequency plasma behavior can be investigated using an MHD model with the addition of the Hall term to the Ohm's law. Such a model embodies some electron dynamics and can therefore be used to investigate physically more complicated processes than a conventional MHD model can. From the modeling standpoint, this model works on the ion time scale and therefore avoids the shorter electron time scale associated with a two-fluid approach. Here, we present one such model with its two as well as three-dimensional versions, test it thoroughly against the linear analytic theory, and finally present an application of the model to the study of the plasma waves generated at a solar wind cometary gas interface.

CONTENTS

INTRODUCTION

Conventional ideal magnetohydrodynamics serves as an excellent tool in investigating low frequency plasma behavior (e.g., $\omega \ll \omega_{ci}$), in which domain both the electrons and the ions can respond to an externally applied electric field and move at the $c\mathbf{E}\times\mathbf{B}/B^2$ velocity. Over distances larger than a Debye length no significant electric fields can exist in a frame of reference moving with the plasma and the electrons and the ions flow together.

The set of electrons and ions together behave mainly as a charge neutral fluid. Any magnetic fields, in the ideal case (e.g., where no resistivity or other dissipation is manifested), become frozen in the fluid and move along with it. In this domain the frequencies are mainly associated with ion inertia and magnetic restoring forces. The electrons move to maintain charge neutrality and by applying this constraint they can be eliminated from the problem.[1]

As one begins to investigate the next higher frequency domain (i.e., where $\omega \sim \omega_{ci}$), one enters a domain in which the ions start to slip across the magnetic field relative to the electrons and the electrons must move along $\mathbf{B}$ to maintain charge neutrality. Thus, as one would expect, the electron and ion fluids no longer flow together and a two-fluid treatment is required. A two-fluid approach suits ones needs. However, if the full electron dynamics are kept, the highest frequencies are the electron cyclotron and plasma frequencies and one is obliged to use correspondingly short time scales; this would limit one to very short time simulations.

It turns out, however, that many important results of the two-fluid model can be obtained from a zero mass electron approximation in which the electrons are always in force balance (no electron oscillations). To achieve this, one must add the Hall term to Ohm's law. Therefore, many important

[1] Electron motion along the magnetic field can be important here.

0021-9991/93 $5.00